01 Nov 2016

First Targeted Search for Gravitational-Wave Bursts from Core-Collapse Supernovae in Data of First-Generation Laser Interferometer Detectors

Benjamin P. Abbott

Marco Cavaglia
Missouri University of Science and Technology, cavagliam@mst.edu

For full list of authors, see publisher's website.

Recommended Citation

B. P. Abbott et al., "First Targeted Search for Gravitational-Wave Bursts from Core-Collapse Supernovae in Data of First-Generation Laser Interferometer Detectors," *Physical Review D*, vol. 94, no. 10, American Physical Society (APS), Nov 2016.
The definitive version is available at https://doi.org/10.1103/PhysRevD.94.102001

First targeted search for gravitational-wave bursts from core-collapse supernovae in data of first-generation laser interferometer detectors

B. P. Abbott *et al.*[*]
(LIGO Scientific Collaboration and Virgo Collaboration)
(Received 25 May 2016; published 15 November 2016)

We present results from a search for gravitational-wave bursts coincident with two core-collapse supernovae observed optically in 2007 and 2011. We employ data from the Laser Interferometer Gravitational-wave Observatory (LIGO), the Virgo gravitational-wave observatory, and the GEO 600 gravitational-wave observatory. The targeted core-collapse supernovae were selected on the basis of (1) proximity (within approximately 15 Mpc), (2) tightness of observational constraints on the time of core collapse that defines the gravitational-wave search window, and (3) coincident operation of at least two interferometers at the time of core collapse. We find no plausible gravitational-wave candidates. We present the probability of detecting signals from both astrophysically well-motivated and more speculative gravitational-wave emission mechanisms as a function of distance from Earth, and discuss the implications for the detection of gravitational waves from core-collapse supernovae by the upgraded Advanced LIGO and Virgo detectors.

DOI: 10.1103/PhysRevD.94.102001

I. INTRODUCTION

Core-collapse supernovae (CCSNe) mark the violent death of massive stars. It is believed that the initial collapse of a star's iron core results in the formation of a proto-neutron star and the launch of a hydrodynamic shock wave. The latter, however, fails to immediately explode the star, but stalls and must be *revived* by a yet-uncertain supernova "mechanism" on a ∼0.5–1 s timescale to explode the star (e.g., Refs. [1–3]). If the shock is not revived, a black hole is formed, and no explosion, or only a very weak explosion, results (e.g., Refs. [4–6]). If the shock is revived, it reaches the stellar surface and produces the spectacular electromagnetic display of a type-II or type-Ib/c supernova. The type classification is based on the explosion light curve and spectrum, which depend largely on the nature of the progenitor star (e.g., Ref. [7]). The time from core collapse to breakout of the shock through the stellar surface and first supernova light is minutes to days, depending on the radius of the progenitor and energy of the explosion (e.g., Refs. [8–10]).

Any core-collapse event generates a burst of neutrinos that releases most of the protoneutron star's gravitational binding energy ($\sim 3 \times 10^{53}$ erg $\approx 0.15 M_\odot c^2$) on a time scale of order 10 seconds. This neutrino burst was detected from SN 1987A and confirmed the basic theory of CCSNe [1,11–13].

Gravitational waves (GWs) are emitted by aspherical mass-energy dynamics that include quadrupole or higher-order contributions. Such asymmetric dynamics are expected to be present in the pre-explosion stalled-shock phase of CCSNe and may be crucial to the CCSN explosion mechanism (see, e.g., Refs. [14–17]). GWs can serve as probes of the magnitude and character of these asymmetries and thus may help in constraining the CCSN mechanism [18–20].

Stellar collapse and CCSNe were considered as potential sources of detectable GWs already for resonant bar detectors in the 1960s [21]. Early analytic and semianalytic estimates of the GW signature of stellar collapse and CCSNe (e.g., Refs. [22–26]) gave optimistic signal strengths, suggesting that first-generation laser interferometer detectors could detect GWs from CCSNe in the Virgo cluster (at distances $D \gtrsim 10$ Mpc). Modern detailed multi-dimensional CCSN simulations (see, e.g., Refs. [20,27–35] and the reviews in Refs. [36–38]) find GW signals of short duration ($\lesssim 1$ s) and emission frequencies in the most sensitive ∼10–2000 Hz band of ground-based laser interferometer detectors. Predicted total emitted GW energies are in the range 10^{-12}–$10^{-8} M_\odot c^2$ for emission mechanisms and progenitor parameters that are presently deemed realistic. These numbers suggest that the early predictions were optimistic and that even second-generation laser interferometers (operating from 2015+) such as Advanced LIGO [39], Advanced Virgo [40], and KAGRA [41] will only be able to detect GWs from very nearby CCSNe at $D \lesssim 1$–100 kpc. Only our own Milky Way and the Magellanic Clouds are within that range. The expected event rate is very low and estimated to be $\lesssim$2–3 CCSNe/100 yr [42–47].

However, there are also a number of analytic and semianalytic GW emission models of more extreme scenarios, involving nonaxisymmetric rotational instabilities, centrifugal fragmentation, and accretion disk instabilities. The emitted GW signals may be sufficiently strong to be detectable to much greater distances of $D \gtrsim 10$–15 Mpc,

[*]Full author given at the end of the article.

perhaps even with first-generation laser interferometers (e.g., Refs. [48–51]). These emission scenarios require special and rare progenitor characteristics, but they cannot presently be strictly ruled out on theoretical grounds. In a sphere of radius ∼15 Mpc centered on Earth, the CCSN rate is $\gtrsim 1/\mathrm{yr}$ [8,52]. This makes Virgo cluster CCSNe interesting targets for constraining extreme GW emission scenarios.

Previous observational constraints on GW burst sources applicable to CCSNe come from all-sky searches for short-duration GW burst signals [53–59]. These searches did not target individual astrophysical events. In addition, a matched-filter search looking for monotonic GW chirps has been performed for the type-Ib/c SN 2010br using publicly released LIGO data [60]; no candidate GW detections were identified. Targeted searches have the advantage over all-sky searches that potential signal candidates in the data streams have to arrive in a well-defined temporal *on-source window* and have to be consistent with coming from the sky location of the source. Both constraints can significantly reduce the noise background and improve the sensitivity of the search (e.g., Ref. [61]). Previous targeted GW searches have been carried out for gamma-ray bursts [62–69], soft gamma repeater flares [70,71], and pulsar glitches [72]. A recent study [73] confirmed that targeted searches with Advanced LIGO and Virgo at design sensitivity should be able to detect neutrino-driven CCSNe out to several kiloparsecs and rapidly rotating CCSNe out to tens of kiloparsecs, while more extreme GW emission scenarios will be detectable to several megaparsecs. An extended analysis [74] of GW spectrograms shows that several characteristic CCSN signal features can be extracted with KAGRA, Advanced LIGO and the Virgo network.

In this paper, we present a targeted search for GWs from CCSNe using the first-generation Initial LIGO (iLIGO) [75], GEO 600 [76], and Virgo [77] laser interferometer detectors. The data searched were collected over 2005–2011 in the S5, A5, and S6 runs of the iLIGO and GEO 600 detectors, and in the VSR1–VSR4 runs of the Virgo detector. From the set of CCSNe observed in this period [78], we make a preliminary selection of four targets for our search: SNe 2007gr, 2008ax, 2008bk, and 2011dh. These CCSNe exploded in nearby galaxies ($D \lesssim 10$ Mpc), have well constrained explosion dates, and have at least partial coverage by coincident observation of more than one interferometer. SNe 2008ax and 2008bk occurred in the astrowatch (A5) period between the S5 and S6 iLIGO science runs. In A5, the principal goal was detector commissioning, not data collection. Data quality and sensitivity were not of primary concern. Preliminary analyses of the gravitational-wave data associated with SNe 2008ax and 2008bk showed that the sensitivity was much poorer than the data for SNe 2007gr and 2011dh. Because of this, we exclude SNe 2008ax and 2008bk and focus our search and analysis on SNe 2007gr and 2011dh. It is also worth mentioning that a matched filter search for a type-Ib/c supernovae GW database was performed on publicly released LIGO data [79] with no detection claimed. The search was not targeted in the sense used here.

We find no evidence for GW signals from SNe 2007gr or 2011dh in the data. Using gravitational waveforms from CCSN simulations, waveforms generated with phenomenological astrophysical models, and *ad hoc* waveforms, we measure the sensitivity of our search. We show that none of the considered astrophysical waveforms would likely be detectable at the distances of SNe 2007gr and 2011dh for the first-generation detector networks. Furthermore, even a very strong gravitational wave could potentially be missed due to incomplete coverage of the CCSN on-source window by the detector network. Motivated by this, we provide a statistical approach for model exclusion by combining observational results for multiple CCSNe. Using this approach, we quantitatively estimate how increased detector sensitivity and a larger sample of targeted CCSNe will improve our ability to rule out the most extreme emission models. This suggests that observations with second-generation "advanced" interferometers [39–41] will be able to put interesting constraints on the GW emission of extragalactic CCSN at $D \lesssim 10$ Mpc.

The remainder of this paper is structured as follows: In Sec. II, we discuss the targeted CCSNe and the determination of their on-source windows. In Sec. III, we describe the detector networks, the coverage of the on-source windows with coincident observation, and the data searched. In Sec. IV, we present our search methodology and the waveform models studied. We present the search results in Sec. V and conclusions in Sec. VI.

II. TARGETED CORE-COLLAPSE SUPERNOVAE

For the present search, it is important to have an estimate of the time of core collapse for each supernova. This time coincides (within one to a few seconds; e.g., Ref. [36]) with the time of strongest GW emission. The better the estimate of the core-collapse time, the smaller the *on-source window* of detector data that must be searched and the smaller the confusion background due to non-Gaussian nonstationary detector noise.

For a Galactic or Magellanic Cloud CCSN, the time of core collapse would be extremely well determined by the time of arrival of the neutrino burst that is emitted coincident with the GW signal [80]. A very small on-source window of seconds to minutes could be used for such a special event.

For CCSNe at distances $D \gtrsim 1$ Mpc, an observed coincident neutrino signal is highly unlikely [81–83]. In this case, the time of core collapse must be inferred based on estimates of the explosion time, explosion energy, and the radius of the progenitor. The explosion time is defined

as the time at which the supernova shock breaks out of the stellar surface and the electromagnetic emission of the supernova begins. Basic information about the progenitor can be obtained from the light curve and spectrum of the supernova (e.g., Ref. [7]). Much more information can be obtained if pre-explosion imaging of the progenitor is available (e.g., Ref. [84]). A red supergiant progenitor with a typical radius of ~ 500–$1500 R_\odot$ produces a type-IIP supernova and has an explosion time of $\sim$1–2 days after core collapse and a typical explosion energy of 10^{51} erg; subenergetic explosions lead to longer explosion times (e.g., Refs. [8–10]). A yellow supergiant that has been partially stripped of its hydrogen-rich envelope, giving rise to a IIb supernova (e.g., Ref. [85]), is expected to have a radius of ~ 200–$500 R_\odot$ and an explosion time of $\lesssim 0.5$ days after core collapse [10,85]. A blue supergiant, giving rise to a peculiar type-IIP supernova (such as SN 1987A), has a radius of $\lesssim 100 R_\odot$ and an explosion time of $\lesssim$2–3 hours after core collapse. A Wolf-Rayet star progenitor, giving rise to a type-Ib/c supernova, has been stripped of its hydrogen (and helium) envelope by stellar winds or binary interactions and has a radius of only a few to $\sim 10 R_\odot$ and shock breakout occurs within $\sim$10–100 s of core collapse [8,9].

The breakout of the supernova shock through the surface of the progenitor star leads to a short-duration high-luminosity burst of electromagnetic radiation with a spectral peak dependent on the radius of the progenitor. The burst from shock breakout precedes the rise of the optical light curve, which occurs on a time scale of days after shock breakout (depending, in detail, on the nature of the progenitor star; Refs. [7,10,85,86]).

With the exception of very few serendipitous discoveries of shock breakout bursts (e.g., Refs. [87,88]), core-collapse supernovae in the 2007–2011 time frame of the present GW search were usually discovered days after explosion, and their explosion time is constrained by one or multiple of (i) the most recent nondetection, i.e., by the last date of observation of the host galaxy without the supernova present; (ii) the comparison of the observed light curve and spectra with those of other supernovae for which the explosion time is well known; (iii) the light-curve extrapolation [89]; or, (iv), for type IIP supernovae, light-curve modeling using the expanding photosphere method (EPM; e.g., Refs. [90,91]).

More than 100 core-collapse supernovae were discovered in the optical by amateur astronomers and professional astronomers (e.g., Ref. [78]) during the S5/S6 iLIGO and the VSR2, VSR3, VSR4 Virgo data-taking periods. In order to select optically discovered core-collapse supernovae as triggers for this search, we impose the following criteria: (i) A distance from Earth not greater than $\sim$10–15 Mpc. Since GWs from core-collapse supernovae are most likely very weak and because the observable GW amplitude scales with 1 over the distance, nearer events are greatly favored. (ii) A well-constrained time of explosion leading to an uncertainty in the time of core collapse of less than $\sim$2 weeks. (iii) At least partial availability of science-quality data of coincident observations of more than one interferometer in the on-source window.

The core-collapse supernovae making these cuts are SN 2007gr, SN 2008ax, SN 2008bk, and SN 2011dh. Table I summarizes key properties of these supernovae, and we discuss each in more detail in the following.

SN 2007gr, a type-Ic supernova, was discovered on 2007 August 15.51 UTC [92]. A prediscovery empty image taken by KAIT [93] on August 10.44 UTC provides a baseline constraint on the explosion time. The progenitor of this supernova was a compact stripped-envelope star [94–97] through which the supernova shock propagated within tens to hundreds of seconds. In order to be conservative, we add an additional hour to the interval between discovery and last nondetection and arrive at a GW on-source window of 2007 August 10.39 UTC to 2007 August 15.51 UTC. The sky location of SN 2007gr is R.A. $= 02^{\mathrm{h}}43^{\mathrm{m}}27^{\mathrm{s}}.98$, Decl $= +37°20'44''.7$ [92]. The host galaxy is NGC 1058. Schmidt *et al.* [98] used EPM to determine the distance to SN 1969L, which exploded in the same galaxy. They found $D = (10.6 + 1.9 - 1.1)$ Mpc. This is broadly consistent with the more recent Cepheid-based distance estimate of $D = (9.29 \pm 0.69)$ Mpc to

TABLE I. Core-collapse supernovae selected as triggers for the gravitational-wave search described in this paper. Distance gives the best current estimate for the distance to the host galaxy. t_1 and t_2 are the UTC dates delimiting the on-source window. Δt is the temporal extent of the on-source window. iLIGO/Virgo run indicates the data-taking campaign during which the supernova explosion was observed. Detectors lists the interferometers taking data during at least part of the on-source window. The last column provides the relative coverage of the on-source window with science-quality or Astrowatch-quality data of at least two detectors. For SN 2007gr, the relative coverage of the on-source window with the most sensitive network of four active interferometers is 67%. See the text in Sec. II for details and references on the supernovae, and see Sec. III for details on the detector networks, coverage, and data quality.

Identifier	Type	Host Galaxy	Distance [Mpc]	t_1 [UTC]	t_2 [UTC]	Δt [days]	iLIGO/Virgo Run	Active Detectors	Coincident Coverage
SN 2007gr	Ic	NGC 1058	10.55 ± 1.95	2007 Aug 10.39	2007 Aug 15.51	5.12	S5/VSR1	H1, H2, L1, V1	93%
SN 2008ax	IIb	NGC 4490	$9.64 + 1.38 - 1.21$	2008 Mar 2.19	2008 Mar 3.45	1.26	A5	G1, H2	8%
SN 2008bk	IIP	NGC 7793	$3.53 + 0.21 - 0.29$	2008 Mar 13.50	2008 Mar 25.14	11.64	A5	G1, H2	38%
SN 2011dh	IIb	M51	8.40 ± 0.70	2011 May 30.37	2011 May 31.89	1.52	S6E/VSR4	G1, V1	37%

NGC 925 by Ref. [99]. This galaxy is in the same galaxy group as NGC 1058 and thus presumed to be in close proximity. For the purpose of the present study, we use the conservative combined distance estimate of $D = (10.55 \pm 1.95\ \mathrm{Mpc})$.

SN 2008ax, a type-IIb supernova [100], was discovered by KAIT on 2008 March 3.45 UTC [101]. The fortuitous nondetection observation made by Arbour on 2008 March 3.19 UTC [102], a mere 6.24 h before the SN discovery, provides an excellent baseline estimate of the explosion time. Spectral observations indicate that the progentior of SN 2008ax was almost completely stripped of its hydrogen envelope, suggesting that is exploded either as a yellow supergiant or as a Wolf-Rayet star [103,104]. Most recent observations and phenomenological modeling by Ref. [105] suggest that the progenitor was in a binary system and may have had a blue-supergiant appearance and an extended $(30\text{–}40R_\odot)$ low-density (thus, low-mass) hydrogen-rich envelope at the time of explosion. To be conservative, we add an additional day to account for the uncertainty in shock propagation time and define the GW on-source window as 2008 March 2.19 UTC to 2008 March 3.45 UTC. The coordinates of SN 2008ax are R.A. $= 12^{\mathrm{h}}30^{\mathrm{m}}40^{\mathrm{s}}.80$, Decl $= +41°38'14''.5$ [101]. Its host galaxy is NGC 4490, which together with NGC 4485 forms a pair of interacting galaxies with a high star formation rate. We adopt the distance $D = (9.64 + 1.38 - 1.21)$ Mpc given by Pastorello *et al.* [106].

SN 2008bk, a type-IIP supernova, was discovered on 2008 March 25.14 UTC [107]. Its explosion time is poorly constrained by a pre-explosion image taken on 2008 January 2.74 UTC [107]. Morrell and Stritzinger [108] compared a spectrum taken of SN 2008bk on 2008 April 12.4 UTC to a library of SN spectra [109] and found a best fit to the spectrum of SN 1999em taken at 36 days after explosion [108]. However, the next other spectra available for SN 1999em are from 20 and 75 days after explosion, so the uncertainty of this result is rather large. EPM modeling by Dessart [110] suggests an explosion time of March 19.5 ± 5 UTC, which is broadly consistent with the light-curve data and hydrodynamical modeling presented in Ref. [111]. The progenitor of SN 2008bk was most likely a red supergiant with a radius of $\sim 500R_\odot$ [112–114], which suggests an explosion time of $\sim$1 day after core collapse [8–10]. Hence, we assume a conservative on-source window of 2008 March 13.5 UTC to 2008 March 25.14 UTC. The coordinates of SN 2008bk are R.A. $= 23^{\mathrm{h}}57^{\mathrm{m}}50^{\mathrm{s}}.42$, Decl $= -32°33'21''.5$ [115]. Its host galaxy is NGC 7793, which is located at a Cepheid distance $D = (3.44 + 0.21 - 0.2)$ Mpc [116]. This distance estimate is consistent with $D = (3.61 + 0.13 - 0.14)$ Mpc obtained by Ref. [117] based on the tip of the red-giant branch method (e.g., Ref. [118]). For the purpose of this study, we use a conservative averaged estimate of $D = (3.53 + 0.21 - 0.29)$ Mpc.

SN 2011dh, a type-IIb supernova, has an earliest discovery date in the literature of 2011 May 31.893, which was by amateur astronomers [119–122]. An earlier discovery date of 2011 May 31.840 is given by Alekseev [123] and a most recent nondetection by Dwyer on 2011 May 31.365 [123]. The progenitor of SN 2011dh was with high probability a yellow supergiant star [124] with a radius of a few $100R_\odot$ [85,125,126]. We conservatively estimate an earliest time of core collapse of a day before the most recent nondetection by Dwyer and use an on-source window of 2011 May 30.365 to 2011 May 31.893. SN 2011dh's location is R.A. $= 13^{\mathrm{h}}30^{\mathrm{m}}05^{\mathrm{s}}.12$, Decl $= +47°10'11''.30$ [127] in the nearby spiral galaxy M51. The best estimates for the distance to M51 come from Vinkó *et al.* [125], who give $D = 8.4 \pm 0.7$ Mpc on the basis of EPM modeling of SN 2005cs and SN 2011dh. This is in agreement with Feldmeier *et al.* [128], who give $D = 8.4 \pm 0.6$ Mpc on the basis of planetary nebula luminosity functions. Estimates using surface brightness variations [129] or the Tully-Fisher relation [130] are less reliable, but give somewhat lower distance estimates of $D = 7.7 \pm 0.9$ and $D = 7.7 \pm 1.3$, respectively. We adopt the conservative distance $D = 8.4 \pm 0.7$ Mpc for the purpose of this study.

III. DETECTOR NETWORKS AND COVERAGE

This search employs data from the 4 km LIGO Hanford, Washington, and LIGO Livingston, Louisiana, interferometers (denoted *H1* and *L1*, respectively), from the 2 km LIGO Hanford, Washington, interferometer (denoted as *H2*), from the 0.6 km GEO 600 detector near Hannover, Germany (denoted as *G1*), and from the 3 km Virgo interferometer near Cascina, Italy (denoted as *V1*).

Table II lists the various GW interferometer data-taking periods ("runs") in the 2005–2011 time frame from which we draw data for our search. The table also provides the duty factor and *coincident* duty factor of the GW interferometers. The duty factor is the fraction of the run time a given detector was taking science-quality data. The coincident duty factor is the fraction of the run time at least two detectors were taking science quality data. The coincident duty factor is most relevant for GW searches like ours that require data from at least two detectors to reject candidate events that are due to non-Gaussian instrumental or environmental noise artifacts ("glitches") but can mimic real signals in shape and time-frequency content (see, e.g., Refs. [57,75]).

One notes from Table II that the duty factor for the first-generation interferometers was typically $\lesssim$50%–80%. The relatively low duty factors are due to a combination of environmental causes (such as distant earthquakes causing loss of interferometer lock) and interruptions for detector commissioning or maintenance.

The CCSNe targeted by this search and described in Sec. II are the only 2007–2011 CCSNe located within

TABLE II. Overview of GW interferometer science runs from which we draw data for our search. H1 and H2 stand for the LIGO Hanford 4 km and 2 km detectors, respectively. L1 stands for the LIGO Livingston detector. V1 stands for the Virgo detector, and G1 stands for the GEO 600 detector. The duty factor column indicates the approximate fraction of science-quality data during the observation runs. The coincident duty factor column indicates the fraction of time during which at least two detectors were taking science-quality data simultaneously. The A5 run was classified as astrowatch and was not a formal science run. The H2 and V1 detectors operated for only part of A5. The Virgo VSR1 run was joint with the iLIGO S5 run, the Virgo VSR2 and VSR3 runs were joint with the iLIGO S6 run, and the GEO 600 detector (G1) operated in iLIGO run S6E during Virgo run VSR4. When iLIGO and Virgo science runs overlap, the coincident duty factor takes into account iLIGO, GEO 600, and Virgo detectors.

Run	Detectors	Run Period	Duty Factors	Coin. Duty Factor
S5	H1, H2, L1, G1	2005/11/04–2007/10/01	∼75% (H1), ∼76% (H2), ∼65% (L1), ∼77% (G1)	∼87%
A5	G1, H2, V1	2007/10/01–2009/05/31	∼81% (G1), ∼18% (H2), ∼5% (V1)	∼18%
S6	L1, H1, G1	2009/07/07–2010/10/21	∼51% (H1), ∼47% (L1), ∼56% (G1)	∼67%
S6E	G1	2011/06/03–2011/09/05	∼77%	∼66%
VSR1/S5	V1	2007/05/18–2007/10/01	∼80%	∼97%
VSR2/S6	V1	2009/07/07–2010/01/08	∼81%	∼74%
VSR3/S6	V1	2010/08/11–2010/10/19	∼73%	∼94%
VSR4/S6E	V1	2011/05/20–2011/09/05	∼78%	∼62%

$D \lesssim 10$–15 Mpc for which well-defined on-source windows exist and which are also covered by extended stretches of coincident observations of at least two interferometers. In Fig. 1, we depict the on-source windows for SNe 2007gr, 2008ax, 2008bk, and 2011dh. We indicate with regions of different color times during which the various interferometers were collecting data.

SN 2007gr exploded during the S5/VSR1 joint run between the iLIGO, GEO 600, and Virgo detectors. It has the best coverage of all considered CCSNe: 93% of its on-source window is covered by science-quality data from at least two of H1, H2, L1, and V1. We search for GWs from SN 2007gr at times when data from the following detector networks are available: H1H2L1V1, H1H2L1, H1H2V1, H1H2, L1V1. The G1 detector was also taking data during SN 2007gr's on-source window, but since its sensitivity was much lower than that of the other detectors, we do not analyze G1 data for SN 2007gr.

SNe 2008ax and 2008bk exploded in the A5 astrowatch run between the S5 and S6 iLIGO science runs (cf. Table II). Only the G1 and H2 detectors were operating at sensitivities much lower than those of the 4 km L1 and H1 and the 3 km V1 detectors. The coincident duty factor for SN 2008ax is only 8%, while that for SN 2008bk is

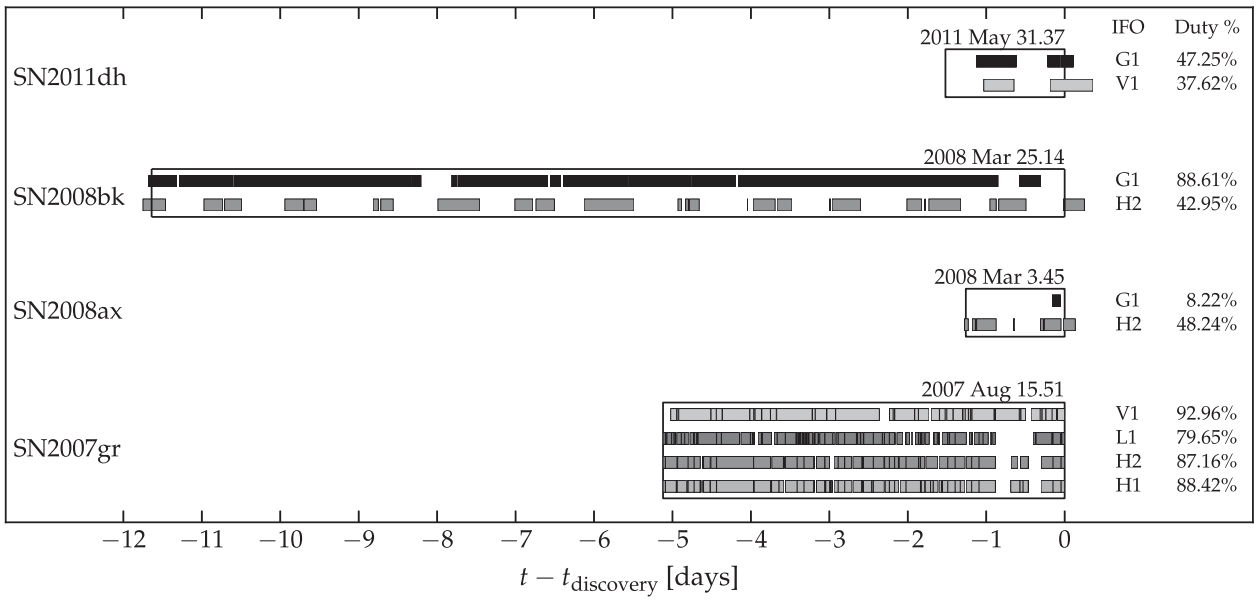

FIG. 1. On-source windows as defined for the four core-collapse supernovae considered in Sec. II. The date given for each core-collapse supernova is the published date of discovery. Overplotted in color are the stretches of time covered with science-quality and Astrowatch-quality data of the various GW interferometers. The percentages given for each core-collapse supernova and interferometer are the fractional coverage of the on-source window with science or astrowatch data by that interferometer. See Table I and Secs. II and III for details.

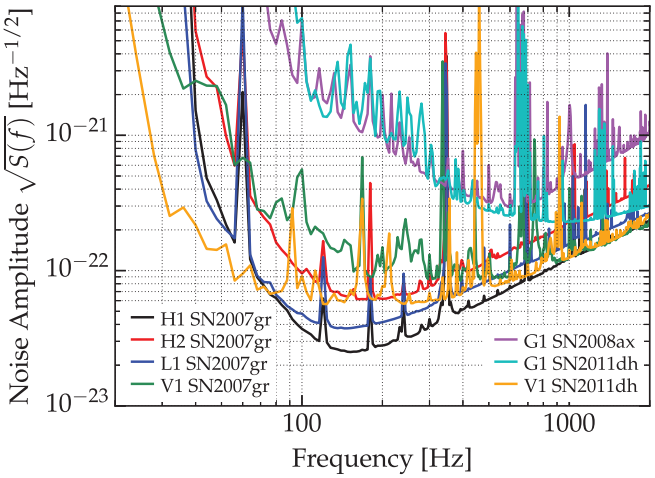

FIG. 2. Noise amplitude spectral densities of the GW interferometers whose data are analyzed for SNe 2007gr and 2011dh (see Sec. III). The curves are the results of averaging $1/S(f)$ over the on-source windows of the SNe (see Table I). We plot the G1 noise spectrum also for SN 2008ax to demonstrate the improvement in high-frequency sensitivity due to GEO-HF [131] for SN 2011dh.

38%. Preliminary analysis of the available coincident GW data showed that due to a combination of low duty factors and low detector sensitivity, the overall sensitivity to GWs from these CCSNe was much lower than for SNe 2007gr and 2011dh. Because of this, we exclude SNe 2008ax and 2008bk from the analysis presented in the rest of this paper.

SN 2011dh exploded a few days before the start of the S6E/VSR4 run during which the V1 and G1 interferometers were operating (cf. Table II). G1 was operating in GEO-HF mode [131], which improved its high-frequency ($f \gtrsim 1$ kHz) sensitivity to within a factor of 2 of V1's sensitivity. While not officially in a science run during the SN 2011dh on-source window, both G1 and V1 were operating and collecting data that passed the data quality standards necessary for being classified as science-quality data (e.g., Refs. [132–134]). The coincident G1V1 duty factor is 37% for SN 2011dh.

In Fig. 2, we plot the one-side noise amplitude spectral densities of each detector averaged over the on-source windows of SNe 2007gr and 2011dh. In order to demonstrate the high-frequency improvement in the 2011 G1 detector, we also plot the G1 noise spectral density for SN 2008ax for comparison.

IV. SEARCH METHODOLOGY

Two search algorithms are employed in this study: X-PIPELINE [61,135] and Coherent WaveBurst (cWB) [136]. Neither algorithm requires detailed assumptions about the GW morphology, and both look for subsecond GW transients in the frequency band 60–2000 Hz. This is the most sensitive band of the detector network, where the amplitude of the noise spectrum of the most sensitive detector is within about an order of magnitude of its minimum. This band also encompasses most models for GW emission from CCSNe (cf. Refs. [36,37,137]). The benefit of having two independent algorithms is that they can act as a cross-check for outstanding events. Furthermore, sensitivity studies using simulated GWs show some complementarity in the signals detected by each pipeline; this is discussed further in Sec. V.

The two algorithms process the data independently to identify potential GW events for each supernova and network combination. Each algorithm assigns a "loudness" measure to each event; these are described in more detail below. The two algorithms also evaluate measures of signal consistency across different interferometers and apply thresholds on these measures (called coherence tests) to reject background noise events. The internal thresholds of each algorithm are chosen to obtain robust performance across a set of signal morphologies of interest. We also reject events that occur at times of environmental noise disturbances that are known to be correlated with transients in the GW data via well-established physical mechanisms; these so-called "category 2" data quality cuts are described in Ref. [58].

The most important measure of an event's significance is its false alarm rate (FAR): the rate at which the background noise produces events of equal or higher loudness than events that pass all coherent tests and data quality cuts. Each pipeline estimates the FAR using background events generated by repeating the analysis on time-shifted data—the data from the different detectors are offset in time, in typical increments of ~1 s. The shifts remove the chance of drawing a subsecond GW transient into the background sample, since the largest time of flight between the LIGO and Virgo sites is 27 milliseconds (between H1 and V1). To accumulate a sufficient sampling of rare background events, this shifting procedure is performed thousands of times without repeating the same relative time shifts among detectors. Given a total duration $T_{\rm off}$ of off-source (time-shifted) data, the smallest false alarm rate that can be measured is $1/T_{\rm off}$.

On-source events from each combination of CCSN, detector network, and pipeline are assigned a FAR using the time-slide background from that combination only. The event lists from the different CCSNe, detector networks, and pipelines are then combined and the events ranked by their FAR. The event with lowest FAR is termed the *loudest event*.

In order for the loudest event to be considered as a GW detection, it must have a false alarm probability (FAP) low enough that it is implausible to have been caused by background noise. Given a FAR value R, the probability $p(R)$ of noise producing one or more events of FAR less than or equal to R during one or more CCSN on-source windows of total duration $T_{\rm on}$ is

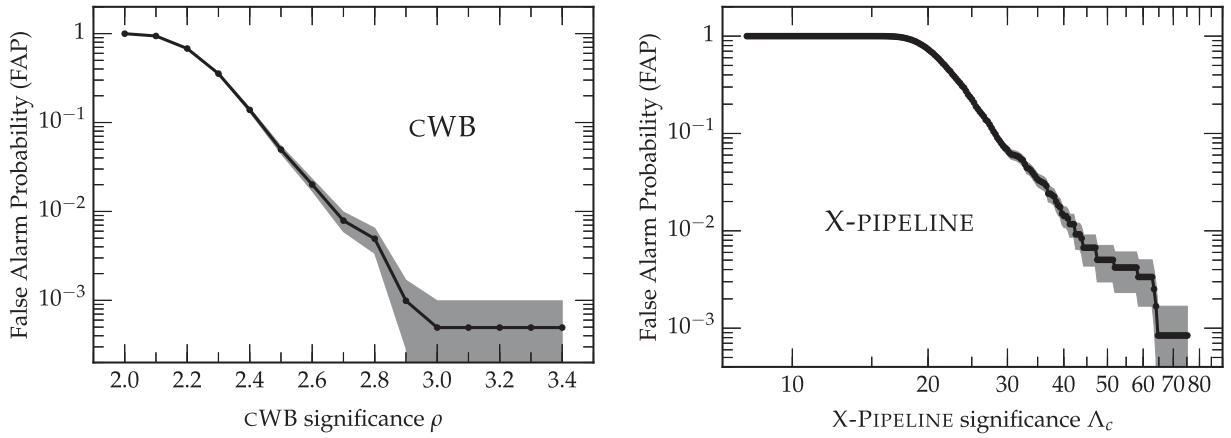

FIG. 3. False Alarm Probability [FAP, Equation (1)] distributions of the background events for SN 2007gr and the H1H2L1V1 detector network (cf. Section III). The FAP indicates the probability that an event of a given "loudness" (significance) is consistent with background noise. The left panel shows the FAP distribution determined by the cWB pipeline as a function of its loudness measure, ρ, (see [136] for details). The right panel depicts the same for X-PIPELINE as a function of its loudness measure, Λ_c, (see [61,135] for details). The shaded regions indicate $1-\sigma$ error estimates for the FAP.

$$p = 1 - \exp(-RT_{\rm on}). \quad (1)$$

The smallest such false alarm probability (FAP) that can be measured given an off-source (time-shifted) data duration $T_{\rm off}$ is approximately $T_{\rm on}/T_{\rm off}$. Several thousand time shifts are therefore sufficient to measure FAP values of $O(10^{-3})$. We require a FAP below 0.001, which exceeds 3σ confidence, in order to consider an event to be a possible GW detection candidate. Figure 3 shows examples of the FAP as a function of event loudness for cWB and X-PIPELINE for the H1H2L1V1 network during the SN 2007gr on-source window.

The loudest surviving events of the current search are reported in Table III. In practice, none of these events has a FAP low enough to be considered a GW candidate (see Sec. V for further discussion). We therefore set upper limits on the strength of possible GW emission by the CCSNe. This is done by adding to the data simulated GW signals of various amplitudes (or equivalently sources at various distances) and repeating the analysis. For each amplitude or distance, we measure the fraction of simulations that produce an event in at least one pipeline with FAP lower than the loudest on-source event, and which survive our coherence tests and data quality cuts; this fraction is the *detection efficiency* of the search.

TABLE III. False alarm rate (FAR) of the loudest event found by each pipeline for each detector network. No on-source events survived the coherent tests and data quality cuts for the cWB analysis of the H1H2L1 and H1H2 networks for SN 2007gr. The lowest FAR, 1.7×10^{-6} Hz, corresponds to a FAP of 0.77, where the total live time analyzed was $T_{\rm on} = 873461$ s.

Network	cWB	X-PIPELINE
H1H2L1V1	1.7×10^{-6} Hz	2.5×10^{-6} Hz
H1H2L1	no events	1.1×10^{-5} Hz
H1H2V1	1.2×10^{-5} Hz	5.3×10^{-6} Hz
H1H2	no events	7.1×10^{-5} Hz
L1V1	4.8×10^{-5} Hz	4.1×10^{-3} Hz
G1V1	1.2×10^{-5} Hz	2.7×10^{-5} Hz

A. Coherent WaveBurst

The cWB [136] analysis is performed as described in Ref. [57], and it is based on computing a constrained likelihood function. In brief, each detector data stream is decomposed into six different wavelet decompositions (each one with different time and frequency resolutions). The data are whitened, and the largest 0.1% of wavelet magnitudes in each frequency bin and decomposition for each interferometer are retained (we call these "black pixels"). We also retain "halo" pixels, which are those that surround each black pixel. In order to choose pixels that are more likely related to a GW transient (*candidate event*), we identify clusters of them. Once all of the wavelet decompositions are projected into the same time-frequency plane, clusters are defined as sets of contiguous retained pixels (black or halo). Only the pixels involved in a cluster are used in the subsequent calculation of the likelihood. These clusters also need to be consistent between interferometers for the tested direction of arrival. For each cluster of wavelets, a Gaussian likelihood function is computed, where the unknown GW is reconstructed with a maximum-likelihood estimator.

The likelihood analysis is repeated over a grid of sky positions covering the range of possible directions to the GW source. Since the sky location of each of the analyzed CCSNe is well known, we could choose to apply this procedure only for the known CCSN sky location.

However, the detector noise occasionally forces the cWB likelihood to peak in a sky location away from the true sky location. As a consequence, some real GW events could be assigned a smaller likelihood value, lowering the capability to detect them. Because of this, we consider triggers that fall within an error region of 0.4° of the known CCSN sky location and that pass the significance threshold, even if they are not at the peak of the cWB reconstructed sky position likelihood. The 0.4° region is determined empirically by trade-off studies between detection efficiency and FAR.

For SN 2011dh, the noise spectra were very different for the G1 and V1 detectors, with the consequence that the network effectively had only one detector at frequencies up to several hundred Hz, and therefore location reconstruction was very poor. As a consequence, we decided to scan the entire sky for candidate events for this CCSN.

The events reported for a given network configuration are internally ranked for detection purposes by cWB using the coherent network amplitude statistic ρ defined in Ref. [138]. Other constraints related to the degree of similarity of the reconstructed signal across different interferometers [the "network correlation coefficient" (cc)] and the ability of the network to reconstruct both polarizations of the GW signal (called *regulators*) are applied to reject background events; these are also described in Ref. [138].

B. X-Pipeline

In the X-Pipeline [61,135,139] analysis, the detector data are first whitened, then Fourier-transformed. A total energy map is made by summing the spectrogram for each detector, and "hot" pixels are identified as the 1% in each detector with the largest total energy. Hot pixels that share an edge or vertex (nearest neighbors and next-nearest neighbors) are clustered. For each cluster, the raw time-frequency maps are recombined in a number of linear combinations designed to give maximum-likelihood estimates of various GW polarizations given the known sky position of the CCSN. The energy in each combination is recorded for each cluster, along with various time-frequency properties of the cluster. The procedure is repeated using a series of Fourier-transform lengths from $1/4$ s, $1/8$ s, …$1/128$ s. Clusters are ranked internally using a Bayesian-inspired estimate Λ_c of the likelihood ratio for a circularly polarized GW, marginalized over the unknown GW amplitude σ_h with a Jeffreys (logarithmic) prior σ_h^{-1}; see Refs. [135,140,141] for details.

When clusters from different Fourier-transform lengths overlap in time-frequency, the cluster with the largest likelihood Λ_c is retained and the rest are discarded. Finally, a postprocessing algorithm tunes and applies a series of pass/fail tests to reject events due to background noise; these tests are based on measures of correlation between the detectors for each cluster. The tuning of these tests is described in detail in Ref. [61]. For more details, see also Ref. [73].

C. Simulated signals and search sensitivity

An important aspect of the GW search presented in this study is to understand how sensitive the GW detector networks are to GWs emitted by the considered CCSNe. We establish sensitivity via Monte Carlo simulation in the following way:

(1) We determine the loudest event in the on-source window that is consistent with the CCSN location (and the angular uncertainty of the search algorithms).
(2) We "inject" (add) theoretical waveforms scaled to a specific distance (or emitted GW energy) every 100 s plus a randomly selected time in $[-10, 10]$ s into the time-shifted background data. We compare the loudness of the recovered injections with the loudest on-source event and record the fraction of the injections that passed the coherent tests and data quality cuts and were louder than the loudest on-source event. This fraction is the *detection efficiency*.
(3) We repeat step 2 for a range of distances (or emitted GW energies) to determine the detection efficiency as a function of distance (or emitted GW energy).

We refer the reader to Ref. [73] for more details on the injection procedure.

In this paper, we employ three classes of GW signals for our Monte Carlo studies: (1) representative waveforms from detailed multidimensional (2D axisymmetric or 3D) CCSN simulations; (2) semianalytic phenomenological waveforms of plausible but extreme emission scenarios; and (3) *ad hoc* waveform models with tuneable frequency content and amplitude to establish upper limits on the energy emitted in GWs at a fixed CCSN distance. We briefly summarize the nature of these waveforms below. We list all employed waveforms in Tables IV and V and summarize their key emission metrics. In particular, we provide the angle-averaged root-sum-squared GW strain,

$$h_{\rm rss} = \sqrt{\int \langle h_+^2(t) + h_\times^2(t)\rangle_\Omega \mathrm{d}t}, \tag{2}$$

and the energy $E_{\rm GW}$ emitted in GWs, using the expressions given in Ref. [73].

1. Waveforms from multidimensional CCSN simulations

Rotation leads to a natural axisymmetric quadrupole (oblate) deformation of the collapsing core. The tremendous acceleration at core bounce and protoneutron star formation results in a strong linearly polarized burst of GWs followed by a ringdown signal. Rotating core collapse is the most extensively studied GW emission process in the CCSN context (see, e.g., Refs. [20,27,145–150] and Refs. [36,37,137] for reviews). For the purpose of this

TABLE IV. Injection waveforms from detailed multidimensional CCSN simulations described in the text. For each waveform, we give the emission type, journal reference, waveform identifier, angle-averaged root-sum-squared strain $h_{\rm rss}$, the frequency $f_{\rm peak}$ at which the GW energy spectrum peaks, the emitted GW energy $E_{\rm GW}$, and available polarizations. See Refs. [73,142] for details.

Emission Type	Ref.	Waveform Identifier	$h_{\rm rss}$ $[10^{-22}$@10 kpc]	$f_{\rm peak}$ [Hz]	$E_{\rm GW}$ $[10^{-9}M_\odot c^2]$	Polarizations
Rotating core collapse	[27]	Dim1-s15A2O05ls	1.052	774	7.685	+
Rotating core collapse	[27]	Dim2-s15A2O09ls	1.803	753	27.873	+
Rotating core collapse	[27]	Dim3-s15A3O15ls	2.690	237	1.380	+
2D convection and SASI	[28]	Yakunin-s15	1.889	888	9.079	+
3D convection and SASI	[30]	Müller1-L15-3	1.655	150	3.741×10^{-2}	+, ×
3D convection and SASI	[30]	Müller2-N20-2	3.852	176	4.370×10^{-2}	+, ×
3D convection and SASI	[30]	Müller3-W15-4	1.093	204	3.247×10^{-2}	+, ×
Protoneutron star pulsations	[36]	Ott-s15	5.465	971	429.946	+

study, we select three representative rotating core-collapse waveforms from the 2D general-relativistic study of Dimmelmeier *et al.* [27]. The simulations producing these waveforms used the core of a $15M_\odot$ progenitor star and the Lattimer-Swesty nuclear equation of state [151]. The waveforms are enumerated by Dim1–Dim3 prefixes and are listed in Table IV. They span the range from moderate rotation (Dim1-s15A2O05ls) to extremely rapid rotation (Dim3-s15A3O15ls). See Ref. [27] for details on the collapse dynamics and GW emission.

In nonrotating or slowly rotating CCSNe, neutrino-driven convection and the standing accretion shock instability (SASI) are expected to dominate the GW emission. GWs from convection/SASI have also been extensively studied in 2D (e.g., Refs. [28,31,35,152–157]) and more recently also in 3D [30,33]. For the present study, we select a waveform from a 2D Newtonian (+ relativistic corrections) radiation-hydrodynamics simulation of a CCSN in a $15M_\odot$ progenitor by Yakunin *et al.* [28]. This waveform also captures the frequency content of more recent 3D waveforms [158,159]. This waveform and its key emission metrics are listed as Yakunin-s15 in Table IV. Note that since the simulation producing this waveform was axisymmetric, only the + polarization is available.

CCSNe in nature are 3D and produce both GW polarizations (h_+ and $h_\times$). Only a few GW signals from 3D simulations are presently available. We draw three waveforms from the work of Müller *et al.* [30]. These and their key GW emission characteristics are listed with Müller1–Müller3 prefixes in Table IV. Waveforms Müller1-L15-3 and Müller2-W15-4 are from simulations using two different progenitor models for a $15M_\odot$ star. Waveform Müller2-N20-2 is from a simulation of a CCSN in a $20M_\odot$ star. Note that the simulations of Müller *et al.* [30] employed an *ad hoc* inner boundary at multiple tens of kilometers. This prevented decelerating convective plumes from reaching

TABLE V. Injection waveforms from phenomenological and *ad hoc* emission models described in the text. For each waveform, we give the emission type, journal reference, waveform identifier, angle-averaged root-sum-squared strain $h_{\rm rss}$, the frequency $f_{\rm peak}$ at which the GW energy spectrum peaks, the emitted GW energy $E_{\rm GW}$, and available polarizations. See Refs. [73,142] for details. As sine-Gaussian waveforms are *ad hoc*, they can be rescaled arbitrarily and do not have a defined physical distance or $E_{\rm GW}$ value.

Emission Type	Ref.	Waveform Identifier	$h_{\rm rss}$ $[10^{-20}$@10 kpc]	$f_{\rm peak}$ [Hz]	$E_{\rm GW}$ $[M_\odot c^2]$	Polarizations
Long-lasting bar mode	[143]	LB1-M0.2L60R10f400t100	1.480	800	2.984×10^{-4}	+, ×
Long-lasting bar mode	[143]	LB2-M0.2L60R10f400t1000	4.682	800	2.979×10^{-3}	+, ×
Long-lasting bar mode	[143]	LB3-M0.2L60R10f800t100	5.920	1600	1.902×10^{-2}	+, ×
Long-lasting bar mode	[143]	LB4-M1.0L60R10f400t100	7.398	800	7.459×10^{-3}	+, ×
Long-lasting bar mode	[143]	LB5-M1.0L60R10f400t1000	23.411	800	7.448×10^{-2}	+, ×
Long-lasting bar mode	[143]	LB6-M1.0L60R10f800t25	14.777	1601	1.184×10^{-1}	+, ×
Torus fragmentation instability	[50]	Piro1-M5.0η0.3	2.550	2035	6.773×10^{-4}	+, ×
Torus fragmentation instability	[50]	Piro2-M5.0η0.6	9.936	1987	1.027×10^{-2}	+, ×
Torus fragmentation instability	[50]	Piro3-M10.0η0.3	7.208	2033	4.988×10^{-3}	+, ×
Torus fragmentation instability	[50]	Piro4-M10.0η0.6	28.084	2041	7.450×10^{-2}	+, ×
sine-Gaussian	[144]	SG1-235HzQ8d9linear	⋯	235	⋯	+
sine-Gaussian	[144]	SG2-1304HzQ8d9linear	⋯	1304	⋯	+
sine-Gaussian	[144]	SG3-235HzQ8d9elliptical	⋯	235	⋯	+, ×
sine-Gaussian	[144]	SG4-1304HzQ8d9elliptical	⋯	1304	⋯	+, ×

small radii and high velocities. As a consequence, the overall GW emission in these simulations peaks at lower frequencies than in simulations that do not employ an inner boundary (cf. Refs. [28,31,33,35]). For example, the expected signal-to-noise ratios of waveforms from the simulations of Ref. [33] are 2–3 times higher than those of Müller *et al.*, so their detectable range should be larger by approximately the same factor.

We also do not include any waveforms from 3D rotating core collapse. However, the study in Ref. [160], which used X-PIPELINE and realistic LIGO noise, did include waveforms from the 3D Newtonian magnetohydrodynamical simulations of Scheidegger *et al.* [161]. The two selected waveforms were for a $15M_\odot$ progenitor star with the Lattimer-Swesty equation of state. These simulations exhibited stronger GW emission, and the detectable range was typically 2–3 times further than for the 2D Dimmelmeier *et al.* waveforms.

In some 2D CCSN simulations [162,163], strong excitations of an $\ell = 1$ g-mode (an oscillation mode with gravity as its restoring force) were observed. These oscillations were found to be highly nonlinear and to couple to GW-emitting $\ell = 2$ modes. The result is a strong burst of GWs that lasts for the duration of the large-amplitude mode excitation, possibly for hundreds of milliseconds [36,48]. More recent simulations do not find such strong g-mode excitations (e.g., Refs. [31,164]). We nevertheless include here one waveform from the simulations of Ref. [163] that was reported by Ott [36]. This waveform is from a simulation with a $15M_\odot$ progenitor and is denoted as Ott-s15 in Table IV.

2. Phenomenological waveform models

In the context of rapidly rotating core collapse, various nonaxisymmetric instabilities can deform the protoneutron star into a triaxial ("bar") shape (e.g., Refs. [150,158,165–169]), potentially leading to extended (∼10 ms–few) and energetic GW emission. This emission occurs at twice the protoneutron star spin frequency, with a 90° phase shift between the plus and cross modes (similar to the waveforms from some more realistic 3D simulations), and with amplitude dependent on the magnitude of the bar deformation [49,150,158]. We use the simple phenomenological bar model described in Ref. [143]. Its parameters are the length of the bar deformation, L, in km; its radius, R, in km; the mass, M, in $M_\odot$, involved in the deformation; and the spin frequency, f, and the duration, t, of the deformation. We select six waveforms as representative examples. We sample the potential parameter space by chosing $M = \{0.2, 1.0\}M_\odot$, $f = \{400, 800\}$ Hz, and $t = \{25, 100, 1000\}$ ms. We list these waveforms as "long-lasting bar mode" in Table V and enumerate them as LB1–LB6. The employed model parameters are encoded in the full waveform name. One notes from Table V that the strength of the bar-mode GW emission is orders of magnitude greater than that of any of the waveforms computed from detailed multidimensional simulations listed in Table IV. We emphasize that the phenomenological bar-mode waveforms should be considered as being at the extreme end of plausible GW emission scenarios. Theoretical considerations (e.g., Ref. [36]) suggest that such strong emission is unlikely to obtain in CCSNe. Observationally, however, having this emission in one or all of the CCSNe has not been ruled out.

We also consider the phenomenological waveform model proposed by Piro and Pfahl [50]. They considered the formation of a dense self-gravitating $M_\odot$-scale fragment in a thick accretion torus around a black hole in the context of collapsar-type gamma-ray bursts. The fragment is driven toward the black hole by a combination of viscous torques and energetic GW emission. This is an extreme but plausible scenario. We generate injection waveforms from this model using the implementation described in Ref. [170]. The model has the following parameters: mass $M_{\rm BH}$ of the black hole in $M_\odot$, a spatially constant geometrical parameter controlling the torus thickness, $\eta = H/r$, where H is the disk scale height and r is the local radius, a scale factor for the fragment mass (fixed at 0.2), the value of the phenomenological α viscosity (fixed at $\alpha = 0.1$), and a starting radius that we fix to be $100r_g = 100GM_{\rm BH}/c^2$. We employ four waveforms, probing black hole masses $M_{\rm BH} = \{5, 10\}M_\odot$ and geometry factors $\eta = \{0.3, 0.6\}$. The resulting waveforms and their key emission metrics are listed as "torus fragmentation instability" and enumerated by Piro1–Piro4 in Table V. The full waveform names encode the particular parameter values used. As in the case of the bar-mode emission model, we emphasize that the torus fragmentation instability also represents an extreme GW emission scenario for CCSNe. It may be unlikely based on theoretical considerations (e.g., Refs. [36,170]), but has not been ruled out observationally.

3. Ad hoc waveforms: Sine-Gaussians

Following previous GW searches, we also employ *ad hoc* sine-Gaussian waveforms to establish frequency-dependent upper limits on the emitted energy in GWs. This also allows us to compare the sensitivity of our targeted search with results from previous all-sky searches for GW bursts (e.g., Refs. [57–59]).

Sine-Gaussian waveforms are, as the name implies, sinusoids in a Gaussian envelope. They are analytic and given by

$$h_+(t) = A\frac{1+\alpha^2}{2}\exp\left(-t^2/\tau^2\right)\sin(2\pi f_0 t), \tag{3}$$

$$h_\times(t) = A\alpha\exp\left(-t^2/\tau^2\right)\cos(2\pi f_0 t). \tag{4}$$

Here, A is an amplitude scale factor, $\alpha = \cos\iota$ is the ellipticity of the waveform with ι being the inclination

angle, f_0 is the central frequency, and $\tau = Q/(\sqrt{2}\pi f_0)$, where Q is the quality factor controlling the width of the Gaussian and thus the duration of the signal. Since the focus of our study is more on realistic and phenomenological waveforms, we limit the set of sine-Gaussian waveforms to four, enumerated SG1–SG4 in Table V. We fix $Q = 8.9$ and study linearly polarized ($\cos\iota = 0$) and elliptically polarized ($\cos\iota$ sampled uniformly on $[-1, 1]$) waveforms at $f = \{235, 1304\}$ Hz. We choose this quality factor and these particular frequencies for comparison with Refs. [57–59].

D. Systematic uncertainties

Our efficiency estimates are subject to a number of uncertainties. The most important of these are calibration uncertainties in the strain data recorded at each detector, and Poisson uncertainties due to the use of a finite number of injections (Monte Carlo uncertainties). We account for each of these uncertainties in the sensitivities reported in this paper.

We account for Poisson uncertainties from the finite number of injections using the Bayesian technique described in Ref. [171]. Specifically, given the total number of injections performed at some amplitude and the number detected, we compute the 90% credible lower bound on the efficiency assuming a uniform prior on [0, 1] for the efficiency. All efficiency curves reported in this paper are therefore actually 90%-confidence-level lower bounds on the efficiency.

Calibration uncertainties are handled by rescaling quoted $h_{\rm rss}$ and distance values following the method in Ref. [56]. The dominant effect is from the uncertainties in the amplitude calibration; these are estimated at approximately 10% for G1, H1, and H2; 14% for L1; and 6%–8% for V1 at the times of the two CCSNe studied [172,173]. The individual detector amplitude uncertainties are combined into a single uncertainty by calculating a combined root-sum-square signal-to-noise ratio and propagating the individual uncertainties assuming each error is independent (the signal-to-noise ratio is used as a proxy for the loudness measures the two pipelines use for ranking events). This combination depends upon the relative sensitivity of each detector, which is a function of frequency, so we compute the total uncertainty at a range of frequencies across our analysis band for each CCSN and select the largest result, 7.6%, as a conservative estimate of the total 1σ uncertainty. This 1σ uncertainty is then scaled by a factor of 1.28 (to 9.7%) to obtain the factor by which our amplitude and distance limits must be rescaled in order to obtain values consistent with a 90%-confidence-level upper limit.

V. SEARCH RESULTS

As discussed in Sec. IV, on-source events from each combination of CCSN, detector network, and pipeline are assigned a false alarm rate by comparing to time-slide background events. Table III lists the FAR values of the loudest event found by each pipeline for each network and CCSN. The lowest FAR, 1.7×10^{-6} Hz, was reported by cWB for the analysis of SN 2007gr with the H1H2L1V1 network. This rate can be converted to a false alarm probability (FAP) using Eq. (1). The total duration of data processed by cWB or X-Pipeline for the two CCSNe was $T_{\rm on} = 873461$ s. Equation (1) then yields a false alarm probability of 0.77 for the loudest event; this is consistent with the event being due to background noise. We conclude that none of the events has a FAP low enough to be considered as a candidate GW detection.

We note that the loudest events reported by cWB and X-Pipeline are both from the analysis of SN 2007gr with the H1H2L1V1 network; this is consistent with chance, as this network combination accounted for more than 60% of the data processed. In addition, the times of the loudest X-Pipeline and cWB events differ by more than a day, so they are not due to a common physical trigger.

A. Detection efficiency vs distance

Given the loudest event, we can compute detection efficiencies for the search following the procedure detailed in Sec. IV C. In brief, we measure the fraction of simulated signals that produce events surviving the coherent tests and data quality cuts and which have a FAR (or equivalently, FAP) lower than the loudest event.

Figures 4 and 5 show the efficiency as a function of distance for the CCSN waveforms from multidimensional simulations and the phenomenological waveforms discussed in Sec. IV C and summarized in Tables IV and V. For SN 2007gr, the maximum distance reach is of order 1 kpc for waveforms from detailed multidimensional CCSN simulations, and from ∼100 kpc to ∼1 Mpc for GWs from the phenomenological models (torus fragmentation instability and long-lived rotating bar mode). The variation in distance reach is due to the different peak emission frequencies of the models and the variation in detector sensitivities with frequency, and is easily understood in terms of the expected signal-to-noise ratio of each waveform relative to the noise spectra of Fig. 2. For example, the distance reach for the Yakunin waveform is similar to those of the Müller waveforms even though the Yakunin energy emission is more than 2 orders of magnitude higher; this is due to the emission being at a much higher frequency, where the detectors are less sensitive. Similarly, of the three Müller waveforms, the distance reach is largest for Müller1 because the peak frequency is 150 Hz, where the LIGO detectors have the best sensitivity.

The distance reaches for SN 2011dh are lower by a factor of several than those for SN 2007gr; this is due to the difference in sensitivity of the operating detectors, as is also evident in Fig. 2. Finally, we note that at small distances, the efficiencies asymptote to the fraction of the on-source

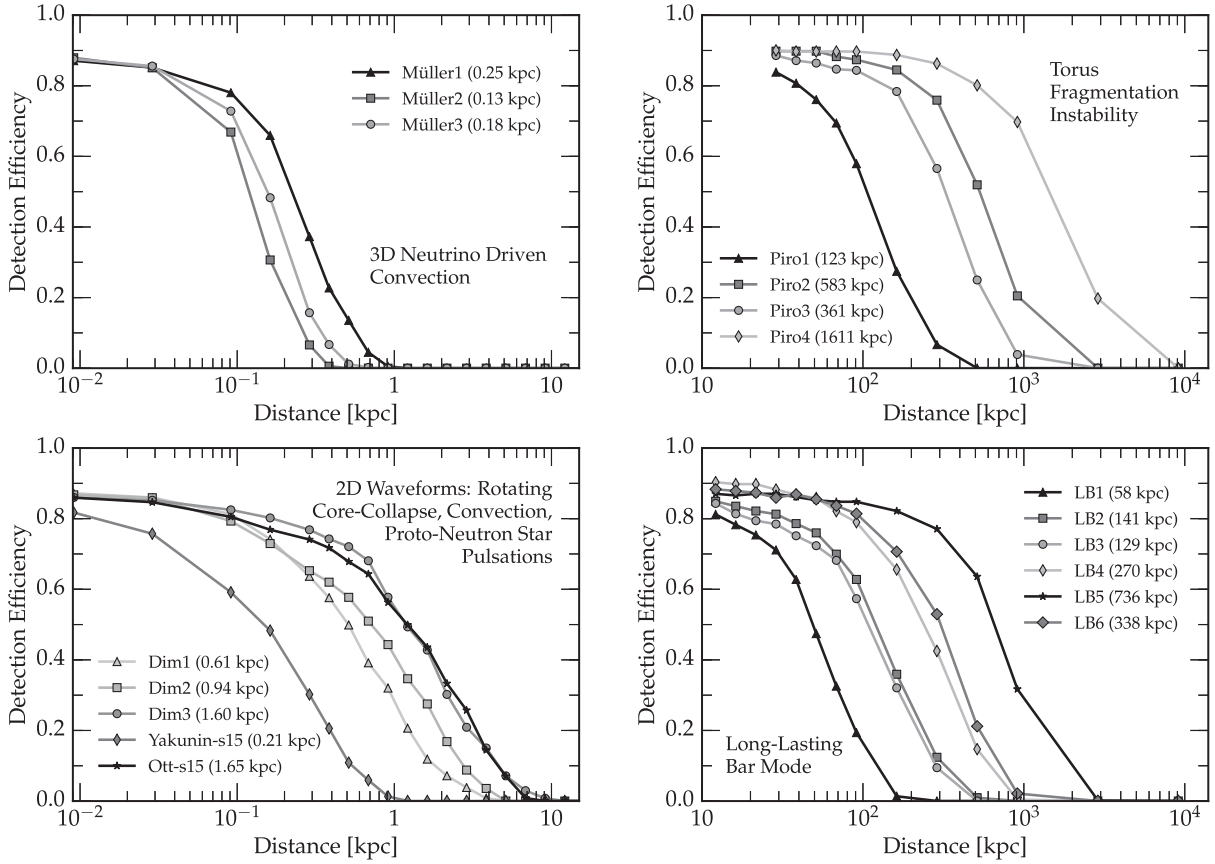

FIG. 4. SN 2007gr detection efficiency versus distance for the waveforms from multidimensional CCSN simulations (left) and the phenomenological waveforms (right) described in Tables IV and V. Simulated GW signals are added into detector data with a range of amplitudes corresponding to different source distances. A simulated signal is considered to be detected if cWB or X-PIPELINE reports an event that survives the coherent tests and data quality cuts with a FAR value lower than that of the loudest event from the SN 2007gr and SN 2011dh on-source windows. These efficiencies are averaged over all detector network combinations for SN 2007gr. The efficiencies are limited to $\leq 93\%$ at small distances due to the fact that this was the duty cycle for coincident observation over the SN 2007gr on-source window. The numbers in brackets for each model are the distances at which the efficiency equals 50% of the asymptotic value at small distances.

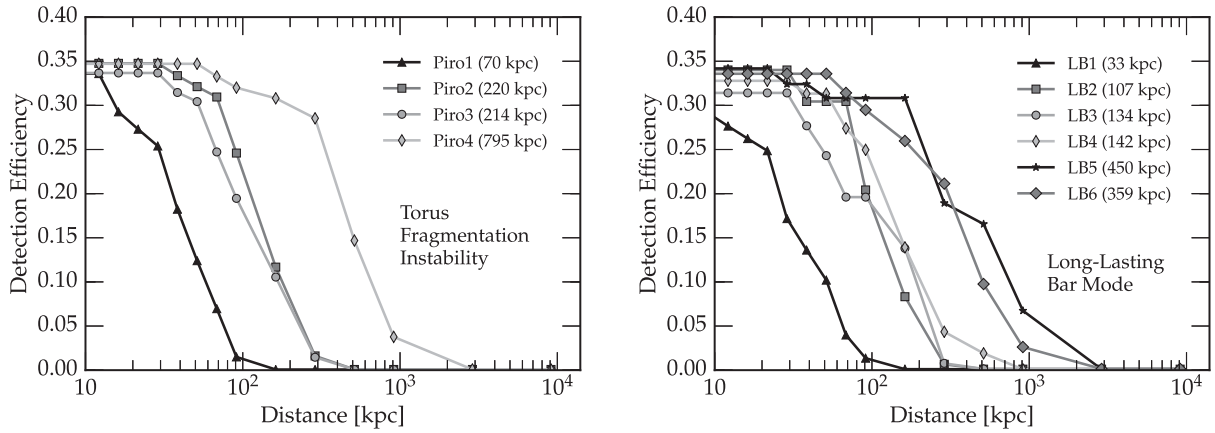

FIG. 5. SN 2011dh detection efficiency vs distance for the phenomenological waveforms described in Table V. Simulated GW signals are added into detector data with a range of amplitudes corresponding to different source distances. A simulated signal is considered to be detected if either cWB or X-PIPELINE reports an event that survives the coherent tests and data quality cuts with a FAR value lower than that of the loudest event from the SN 2007gr and SN 2011dh on-source windows. The efficiencies are limited to $\leq 37\%$ at small distances due to the fact that this was the duty cycle for coincident observation over the SN 2011dh on-source window; some simulations are also vetoed by data quality cuts. The numbers in the brackets are the distances at which the efficiency equals 50% of its maximum value for each model.

window that is covered by coincident data, approximately 93% for SN 2007gr and 37% for SN 2011dh (up to a few percent of simulated signals are lost due to random coincidence with data quality cuts).

We do not show the efficiencies for the multidimensional simulation CCSN waveforms for SN 2011dh, as the detection efficiency was negligible in this case. This is due to the fact that the relative orientation of the G1 and V1 detectors—rotated approximately 45° with respect to each other—means that the two detectors are sensitive to orthogonal GW polarizations. In order for the coherent cuts to reject background noise, X-PIPELINE needs to assume some relationship between these two polarizations. We require that the h_+ and $h_\times$ polarizations be out of phase by 90°, as would be expected for emission from a rotating body with a nonaxisymmetric quadrupole deformation. We choose this because the strongest GW emission models are for rotating nonaxisymmetric systems (the fragmentation instability and long-lived bar mode). Unfortunately, the waveforms from multidimensional CCSN simulations either are linearly polarized (i.e., they have only one polarization) or exhibit randomly changing phase. Hence, they cannot be detected by the search performed for SN 2011dh with X-PIPELINE. The tuning of CWB did not use these constraints; however, the G1 noise floor was about a factor of 2 higher than V1 around 1000 Hz, and the difference was even greater at lower frequencies. This issue weakened the internal CWB measures of correlation of the reconstructed signal between the two interferometers and severely reduced the detection efficiencies at distances beyond a few parsecs.

The distances shown in Fig. 4 and 5 show the probability of a GW signal producing an event with a FAP lower than that of the loudest event. The physical interpretation of the efficiency ϵ at a distance d for a given model is related to the prospect of excluding the model with observations. Explicitly, the nonobservation of any events with FAP lower than the loudest event gives a frequentist exclusion of that GW emission model for a source at distance d with confidence ϵ. However, in this search the loudest event had a large FAP (0.77). In order for an event to be considered as a possible detection, it would need to have a FAP of order 10^{-3} or less; we find that imposing this more stringent requirement lowers the maximum distance reach by approximately 5%–25% depending on the waveform model.

Unfortunately, none of the models have distance reaches out to the ∼10 Mpc distance of SN 2007gr or SN 2011dh; we conclude that our search is not able to constrain the GW emission model for either of these CCSNe.

B. Constraints on energy emission

In addition to the astrophysically motivated phenomenological and multidimensional CCSN simulation waveforms, we employ the *ad hoc* sine-Gaussian waveforms specified by Eqs. (3) and (4) to establish frequency-dependent upper limits on the emitted energy in GWs. This also allows us to compare the sensitivity of our targeted search with results from previous all-sky searches for GW bursts (e.g., Refs. [57–59]).

The detection efficiency is computed using the same procedure as for the other waveforms. However, since these *ad hoc* waveforms have no intrinsic distance scale, we measure the efficiency as a function of the root-sum-square amplitude $h_{\rm rss}$, defined by Eq. (2). For this study, we use the two sine-Gaussian waveforms described in Sec. IV C, which have central frequencies of 235 Hz and 1304 Hz. These are standard choices for all-sky burst searches [59]. Table VI lists the $h_{\rm rss}$ values at which the efficiency reaches half of its maximum value. Note that we use the half-maximum efficiency rather than 50% efficiency here, since the maximum efficiency is limited by the fraction of the on-source window that is covered by coincident data. The half-maximum gives a measure of the distance reach of the instruments independent of their duty cycle.

These $h_{\rm rss}$ values can be converted to limits on energy emission by assuming a specific angular emission pattern of the source [174]. For simplicity, we assume isotropic emission, for which

$$E_{\rm GW} = \frac{\pi^2 c^3}{G} D^2 f_0^2 h_{\rm rss}^2. \tag{5}$$

Here f_0 is the peak frequency of the GW and D is the distance of the source. We use distances of 10.55 Mpc for SN 2007gr and 8.40 Mpc for SN 2011dh. Table VI also lists the energy emission values at which the efficiency reaches half of its maximum value. If the total amount of energy

TABLE VI. Gravitational-wave energy emission constraints at half-maximum detection efficiency for SN 2007gr and SN 2011dh. These assume distances of 10.55 Mpc for SN 2007gr and 8.40 Mpc for SN 2011dh.

	SN 2007gr			SN 2011dh		
Waveform	$h_{\rm rss}$ [Hz$^{-1/2}$]	$E_{\rm GW}$[erg]	$E_{\rm GW}[M_\odot c^2]$	$h_{\rm rss}$ [Hz$^{-1/2}$]	$E_{\rm GW}$[erg]	$E_{\rm GW}[M_\odot c^2]$
SGel2 SG235Q9	5.4×10^{-22}	6.7×10^{52}	0.038	9.1×10^{-21}	1.2×10^{55}	6.8
SGlin2 SG235Q9	6.6×10^{-22}	1.0×10^{53}	0.058	4.8×10^{-20}	3.4×10^{56}	1.9×10^{2}
SGel2 SG1304Q9	2.1×10^{-21}	3.1×10^{55}	17	2.2×10^{-21}	2.3×10^{55}	13
SGlin2 SG1304Q9	2.5×10^{-21}	4.6×10^{55}	26	n/a	n/a	n/a

emitted in GWs was larger than the numbers quoted in the table, we would have had a greater than 50% chance of seeing a signal from the CCSN at the estimated distance, provided coincident observation with the most sensitive detector network. Note, however, that the on-source window did not have 100% coverage (see Sec. III).

The most stringent constraints are a few percent of a mass-energy equivalent of a solar mass emitted in GWs at 235 Hz, where the noise floor is low. The 1304 Hz results indicate that with this data set, we should not expect to be able to detect extragalactic GWs at kHz frequencies, since the limits are less stringent, $O(10)M_{\odot}c^2$ or more.

The above results can be compared with the energy available in CCSNe, which are powered by the gravitational energy released in core collapse. The total available energy is set by the binding energy of a typical $1.4M_{\odot}$ neutron star and is roughly 3×10^{53} erg, corresponding to $\sim 0.15M_{\odot}c^2$ (e.g., Ref. [175]). The observation of neutrinos from SN 1987A confirmed that ~99% of that energy is emitted in the form of neutrinos in protoneutron star cooling (e.g., Ref. [176]). The typical CCSN explosion kinetic energy is $\sim 10^{51}$ erg ($\sim 10^{-3}M_{\odot}c^2$). Considering these observational constraints, the energy emitted in GWs is unlikely to exceed $O(10^{-3})M_{\odot}c^2$. Hence, the energy constraints obtained by this search for SNe 2007gr and 2011dh are not astrophysically interesting.

C. Model exclusion confidence

As we have seen, it is unlikely that we will have coincident science-quality data covering an entire multiday on-source window for any given CCSN. In the present analysis, the coverage of the on-source windows is approximately 93% for SN 2007gr and 37% for SN 2011dh. Considering that data-quality cuts typically remove another few percent of live time, we cannot expect to exclude even fairly strong GW emission at the 90% confidence level for a single CCSN. However, by combining observations of multiple CCSNe, it is straightforward to exclude the simple model in which all CCSNe produce identical GW signals; i.e., assuming *standard candle* emission.

Consider a CCSN model M_{SN} which predicts a particular GW emission pattern during the CCSN event (e.g., one of the waveforms considered in Sec. IV C). In the case that no GW candidates are observed, we can constrain that model using observations from multiple CCSN events at known distances d_i using the measured detection efficiencies $\epsilon_i(d_i)$ for each supernova (e.g., as in Fig. 4). These $\epsilon_i(d_i)$ can be combined into an overall model exclusion probability [177], P_{excl}:

$$P_{\mathrm{excl}} = 1 - \prod_{i=1}^{N}(1 - \epsilon_i(d_i)). \tag{6}$$

It is also straightforward to marginalize over uncertainties in the d_i (as in Table I) by the replacement

$$\epsilon_i(d_i) \to \epsilon_i \equiv \int_0^{\infty} d\bar{d}\pi_i(\bar{d})\epsilon_i(\bar{d}), \tag{7}$$

where π_i is our prior on the distance to CCSN i (e.g., a Gaussian).

In the light of the measured sensitivity ranges in Figs. 4 and 5, it is clear that we cannot exclude any of the considered models of GW emission for SN 2007gr and SN 2011dh with the current data. However, LIGO and Virgo are being upgraded to advanced configurations, with a final design sensitivity approximately a factor of 10 better than for the period 2005–2011 considered in this paper. It is therefore instructive to consider what model exclusion statements the advanced detectors will be able to make using future CCSNe similar to SN 2007gr and SN 2011dh. The extrapolation of our results to Advanced LIGO/Advanced Virgo design sensitivity indicates that waveforms predicted by multidimensional CCSN simulations will be individually detectable only to distances of $O(10)$ kpc; the detection of such signals at Mpc distances will require third-generation detectors. We therefore focus on the phenomenological waveform models of plausible but more extreme GW emission, where we expect to reach sooner large standard candle model exclusion probabilities. Specifically, we analyze the rotating bar and torus fragmentation scenarios (see also the discussion in Ref. [73]).

Figure 6 presents model exclusion confidence plots for four of the phenomenological waveform models. These plots are based on the measured efficiencies for SN 2007gr and SN 2011dh, but assume the detector noise spectra have been lowered by a factor of A, so the search would be expected to have the same efficiency for a particular source at A times the distance, and the number of CCSNe in the sample has been increased by a factor of p. For example, $A = 10$ represents having a sensitivity 10 times better than the 2005–2011 data, which is realistic for Advanced LIGO and Advanced Virgo, while $p = 2$ corresponds to having two CCSNe similar to SN 2007gr and two similar to SN 2011dh. The curves correspond to the experimentally derived values based on the 2005–2011 data set. It is worth stressing that the power of excluding models from this data set almost exclusively originates from SN 2007gr, given the more sensitive interferometers available at the time of that supernova. For example, in the bottom-left panel of Fig. 6, the curves, when A is smaller than 9, depend almost exclusively on the contribution of SN 2007gr. In this regard, the presented model exclusion probabilities will be reached with less than $2p$ CCSNe if the sample contains more data sets comparable in coverage and sensitivity to the rescaled SN 2007gr data set than a rescaled SN 2011dh data set. In summary, Fig. 6 shows that it is a reasonable expectation that extended coincident

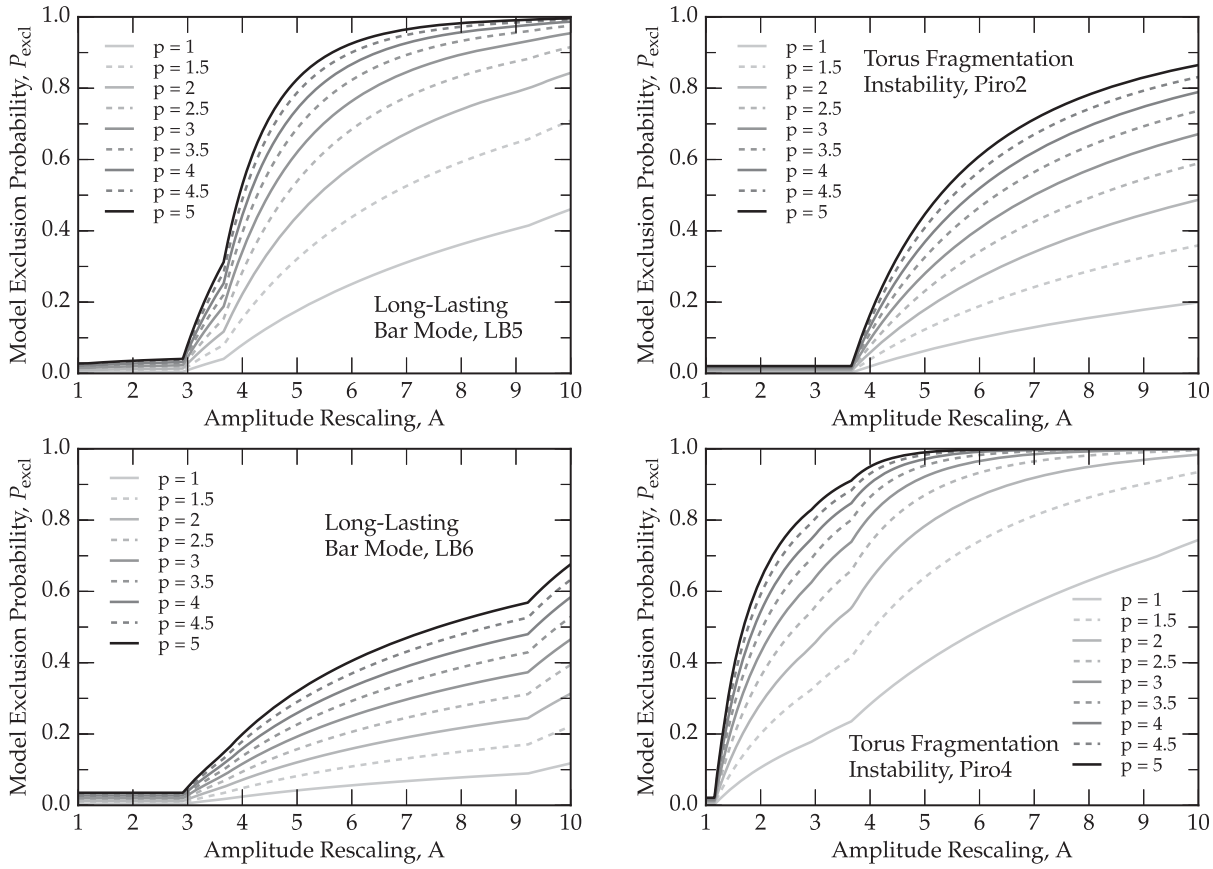

FIG. 6. Expected model exclusion probabilities for example waveforms as a function of amplitude sensitivity rescaling, A, and supernova sample size rescaling, p, based on the SN 2007gr and SN 2011dh sample (e.g. $p = 5$ corresponds to 10 supernovae). The naming convention is described in Table V. Currently none of the emission models can be excluded, but for the advanced detectors with better sensitivity and more nearby CCSNe it is realistic to expect to rule out some of the extreme emission models.

observations with advanced-generation detectors will rule out extreme CCSN emission models.

D. Sensitivity advantage of the triggered search

As noted in Sec. I, targeted searches have the advantage over all-time all-sky searches that potential signal candidates in the data streams have to arrive in a well-defined temporal on-source window and have to be consistent with coming from the sky location of the source. Both constraints can significantly reduce the noise background. Here we assess the improved sensitivity of a triggered search by comparing our h_{rss} sensitivities to linearly polarized sine-Gaussian waveforms for SN 2007gr to those of an all-sky search of the same data.

The most straightforward way to compare two searches is to fix the FAR threshold and compare the h_{rss} values at 50% efficiency. The S5/VSR1 all-sky all-time search [58] using cWB was run on 68.2 days of coincident H1H2L1V1 data with thresholds to give a FAP of 0.1 or less in the frequency band up to 2000 Hz. The live time for the cWB SN 2007gr analysis of the H1H2L1V1 network was 3.25 days, so a FAP of 0.1 corresponds to a FAR of 3.56×10^{-7} Hz. Including calibration and Monte Carlo uncertainties, the h_{rss} values at 50% efficiency for this FAR are 5.0×10^{-22} $\mathrm{Hz}^{-1/2}$ at 235 Hz and 2.2×10^{-21} $\mathrm{Hz}^{-1/2}$ at 1304 Hz. After adjusting for systematic differences in the antenna responses and noise spectra[1] between the S5/VSR1 all-sky search and the SN 2007gr search, the effective all-sky h_{rss} values are 7.0×10^{-22} $\mathrm{Hz}^{-1/2}$ at 235 Hz and 2.9×10^{-21} $\mathrm{Hz}^{-1/2}$ at 1304 Hz, approximately 30% to 40% higher than the targeted search. Equivalently, the distance reach of our targeted search is larger than that of the all-time all-sky search by 30% to 40% at this FAP.

Alternatively, we can compare the two searches without adjusting to a common FAR. After allowing for systematic differences in the antenna responses and noise spectra between the S5/VSR1 all-sky search and the SN 2007gr search, we find that the h_{rss} values at 50% efficiency are identical (to within a few percent). However, the FAR of the SN 2007gr search is lower by an order of magnitude:

[1]In particular, during the on-source window of SN 2007gr, the noise spectral density for L1 was about 50% worse at low frequencies than the average value during the whole of S5.

1.8×10^{-9} Hz compared to 1.7×10^{-8} Hz for the all-sky search. This is consistent with expectations for restricting from an all-sky search to a single sky-position search. Furthermore, the FAP for a trigger produced by the SN 2007gr search will be smaller than that of a trigger from the all-sky search at the same FAR, because the SN 2007gr on-source window (3.5 days for cWB and X-Pipeline combined) is a factor of 20 shorter than the all-sky window (68.2 days). So if we consider a surviving trigger that is just above threshold in the two searches, the SN 2007gr trigger will have an FAP a factor of approximately 200 lower than an all-sky trigger with the same $h_{\rm rss}$.

VI. SUMMARY AND DISCUSSION

We presented the results of the first LIGO-GEO-Virgo search for gravitational-wave (GW) transients in coincidence with optically detected core-collapse supernovae (CCSNe) observed between 2007 and 2011. Two CCSNe, SN 2007gr and SN 2011dh, satisfied our criteria of proximity, well-constrained time of core collapse, and occurrence during times of coincident high-sensitivity operation of at least two GW detectors. No statistically significant GW events were observed associated with either CCSN.

We quantified the sensitivity of the search as a function of distance to the CCSNe using representative waveforms from detailed multidimensional CCSN simulations and from semianalytic phenomenological models of plausible but extreme emission scenarios. The distances out to which we find signals detectable for SNe 2007gr and 2011dh range from $O(\lesssim 1)$ kpc for waveforms from detailed simulations to $O(1)$ Mpc for the more extreme phenomenological models. From the known distances of our two target supernovae, we estimated the minimum energy in gravitational waves corresponding to our sensitivity limits using *ad hoc* sine-Gaussian waveforms. These range from $O(0.1)M_{\odot}c^2$ at low frequencies to $\gtrsim O(10)M_{\odot}c^2$ above 1 kHz.

This first search for GWs from extragalactic CCSNe places the most stringent observational constraints to date on GW emission in core-collapse supernovae. A comparison of our search's sensitivity with the standard all-sky, all-time search for generic GW bursts in the same GW detector data shows a 35%–40% improvement in distance reach at fixed false alarm probability. This improvement comes from knowledge of the sky positions of the CCSNe and approximate knowledge of the collapse times. It is, hence, clearly beneficial to carry out targeted searches for GWs from CCSNe.

The results of our search do not allow us to exclude astrophysically meaningful GW emission scenarios. We have extrapolated our results to the sensitivity level expected for Advanced LIGO and Virgo. Considering the improved detector sensitivity and assuming the analysis of multiple CCSNe, we find that at design sensitivity (c. 2019, Ref. [178]), this network will be able to constrain the extreme phenomenological emission models for extragalactic CCSNe observed out to distances of ∼10 Mpc. Detection of the most realistic GW signals predicted by multidimensional CCSN simulations will require a Galactic event even at the design sensitivity of the advanced detectors. These are consistent with the results of the study in Ref. [73], which used data from iLIGO and Virgo recolored to match the advanced detector design sensitivities. We conclude that third-generation detectors with a sensitivity improvement of a factor of 10–20 over the Advanced detectors may be needed to observe GWs from extragalactic CCSNe occurring at a rate of 1–2 per year within ∼10 Mpc.

ACKNOWLEDGMENTS

We thank L. Dessart for applying the expanding photosphere method to SN 2008bk to derive an approximate explosion date and A. Howell for access to his supernova spectra fit software SUPERFIT. The authors gratefully acknowledge the support of the United States National Science Foundation for the construction and operation of the LIGO Laboratory, the Science and Technology Facilities Council of the United Kingdom, the Max-Planck-Society, and the State of Niedersachsen/Germany for support of the construction and operation of the GEO 600 detector, and the Italian Istituto Nazionale di Fisica Nucleare and the French Centre National de la Recherche Scientifique for the construction and operation of the Virgo detector. The authors also gratefully acknowledge the support of the research by these agencies and by the Australian Research Council, the Council of Scientific and Industrial Research of India, the Istituto Nazionale di Fisica Nucleare of Italy, the Spanish Ministerio de Educación y Ciencia, the Conselleria d'Economia Hisenda i Innovació of the Govern de les Illes Balears, the Foundation for Fundamental Research on Matter supported by the Netherlands Organisation for Scientific Research, the Polish Ministry of Science and Higher Education, the FOCUS Programme of Foundation for Polish Science, the Royal Society, the Scottish Funding Council, the Scottish Universities Physics Alliance, the National Aeronautics and Space Administration, the Carnegie Trust, the Leverhulme Trust, the David and Lucile Packard Foundation, the Research Corporation, and the Alfred P. Sloan Foundation. This document has been assigned LIGO Laboratory document No. LIGO-P1400208.

[1] H. A. Bethe, Rev. Mod. Phys. **62**, 801 (1990).
[2] H.-T. Janka, Annu. Rev. Nucl. Part. Sci. **62**, 407 (2012).
[3] A. Burrows, Rev. Mod. Phys. **85**, 245 (2013).
[4] E. O'Connor and C. D. Ott, Astrophys. J. **730**, 70 (2011).
[5] E. Lovegrove and S. E. Woosley, Astrophys. J. **769**, 109 (2013).
[6] A. L. Piro, Astrophys. J. Lett. **768**, L14 (2013).
[7] A. V. Filippenko, Annu. Rev. Astron. Astrophys. **35**, 309 (1997).
[8] M. D. Kistler, W. C. Haxton, and H. Yüksel, Astrophys. J. **778**, 81 (2013).
[9] C. D. Matzner and C. F. McKee, Astrophys. J. **510**, 379 (1999).
[10] V. Morozova, A. L. Piro, M. Renzo, C. D. Ott, D. Clausen, S. M. Couch, J. Ellis, and L. F. Roberts, Astrophys. J. **814**, 63 (2015).
[11] W. Baade and F. Zwicky, Proceedings of the Indian National Science Academy Part B, Biological sciences **20**, 254 (1934).
[12] K. Hirata, T. Kajita, M. Koshiba, M. Nakahata, and Y. Oyama, Phys. Rev. Lett. **58**, 1490 (1987).
[13] R. M. Bionta, G. Blewitt, C. B. Bratton, D. Casper, and A. Ciocio, Phys. Rev. Lett. **58**, 1494 (1987).
[14] A. Burrows, J. Hayes, and B. A. Fryxell, Astrophys. J. **450**, 830 (1995).
[15] M. Herant, Phys. Rep. **256**, 117 (1995).
[16] S. M. Couch and C. D. Ott, Astrophys. J. **799**, 5 (2015).
[17] E. J. Lentz, S. W. Bruenn, W. R. Hix, A. Mezzacappa, O. E. B. Messer, E. Endeve, J. M. Blondin, J. A. Harris, P. Marronetti, and K. N. Yakunin, Astrophys. J. Lett. **807**, L31 (2015).
[18] C. D. Ott, Classical Quantum Gravity **26**, 204015 (2009).
[19] J. Logue, C. D. Ott, I. S. Heng, P. Kalmus, and J. Scargill, Phys. Rev. D **86**, 044023 (2012).
[20] E. Abdikamalov, S. Gossan, A. M. DeMaio, and C. D. Ott, Phys. Rev. D **90**, 044001 (2014).
[21] J. Weber, Phys. Rev. Lett. **17**, 1228 (1966).
[22] R. Ruffini and J. A. Wheeler, in *Proceedings of the Conference on Space Physics, ESRO, Paris, France*, edited by V. Hardy and H. Moore (1971), p. 45.
[23] R. A. Saenz and S. L. Shapiro, Astrophys. J. **229**, 1107 (1979).
[24] T. X. Thuan and J. P. Ostriker, Astrophys. J. Lett. **191**, L105 (1974).
[25] J. R. Ipser and R. A. Managan, Astrophys. J. **282**, 287 (1984).
[26] K. S. Thorne, in *300 Years of Gravitation*, edited by S. W. Hawking and W. Israel (Cambridge University Press, Cambridge, UK, 1987).
[27] H. Dimmelmeier, C. D. Ott, A. Marek, and H.-T. Janka, Phys. Rev. D **78**, 064056 (2008).
[28] K. N. Yakunin, P. Marronetti, A. Mezzacappa, S. W. Bruenn, C.-T. Lee, M. A. Chertkow, W. R. Hix, J. M. Blondin, E. J. Lentz, B. Messer *et al.*, Classical Quantum Gravity **27**, 194005 (2010).
[29] C. D. Ott, C. Reisswig, E. Schnetter, E. O'Connor, U. Sperhake, F. Löffler, P. Diener, E. Abdikamalov, I. Hawke, and A. Burrows, Phys. Rev. Lett. **106**, 161103 (2011).
[30] E. Müller, H.-T. Janka, and A. Wongwathanarat, Astron. Astrophys. **537**, A63 (2012).
[31] B. Müller, H.-T. Janka, and A. Marek, Astrophys. J. **766**, 43 (2013).
[32] C. D. Ott, E. Abdikamalov, E. O'Connor, C. Reisswig, R. Haas, P. Kalmus, S. Drasco, A. Burrows, and E. Schnetter, Phys. Rev. D **86**, 024026 (2012).
[33] C. D. Ott, E. Abdikamalov, P. Mösta, R. Haas, S. Drasco, E. P. O'Connor, C. Reisswig, C. A. Meakin, and E. Schnetter, Astrophys. J. **768**, 115 (2013).
[34] T. Kuroda, T. Takiwaki, and K. Kotake, Phys. Rev. D **89**, 044011 (2014).
[35] K. N. Yakunin, A. Mezzacappa, P. Marronetti, S. Yoshida, S. W. Bruenn, W. R. Hix, E. J. Lentz, O. E. B. Messer, J. A. Harris, E. Endeve *et al.*, Phys. Rev. D **92**, 084040 (2015).
[36] C. D. Ott, Classical Quantum Gravity **26**, 063001 (2009).
[37] K. Kotake, C.R. Phys. **14**, 318 (2013).
[38] C. Fryer and K. C. B. New, Living Rev. Relativ. **14**, 1 (2011).
[39] J. Aasi *et al.* (LIGO Scientific Collaboration), Classical Quantum Gravity **32**, 074001 (2015).
[40] F. Acernese *et al.* (Virgo Collaboration), Classical Quantum Gravity **32**, 024001 (2015).
[41] Y. Aso, Y. Michimura, K. Somiya, M. Ando, O. Miyakawa, T. Sekiguchi, D. Tatsumi, and H. Yamamoto (KAGRA Collaboration), Phys. Rev. D **88**, 043007 (2013).
[42] S. van den Bergh and G. A. Tammann, Annu. Rev. Astron. Astrophys. **29**, 363 (1991).
[43] E. Cappellaro, M. Turatto, S. Benetti, D. Y. Tsvetkov, O. S. Bartunov, and I. N. Makarova, Astron. Astrophys. **273**, 383 (1993).
[44] G. A. Tammann, W. Loeffler, and A. Schroeder, Astrophys. J. Suppl. Ser. **92**, 487 (1994).
[45] W. Li, J. Leaman, R. Chornock, A. V. Filippenko, D. Poznanski, M. Ganeshalingam, X. Wang, M. Modjaz, S. Jha, R. J. Foley *et al.*, Mon. Not. R. Astron. Soc. **412**, 1441 (2011).
[46] R. Diehl, H. Halloin, K. Kretschmer, G. G. Lichti, V. Schönfelder, A. W. Strong, A. von Kienlin, W. Wang, P. Jean, J. Knödlseder *et al.*, Nature (London) **439**, 45 (2006).
[47] D. Maoz and C. Badenes, Mon. Not. R. Astron. Soc. **407**, 1314 (2010).
[48] C. D. Ott, A. Burrows, L. Dessart, and E. Livne, Phys. Rev. Lett. **96**, 201102 (2006).
[49] C. Fryer, D. Holz, and S. Hughes, Astrophys. J. **565**, 430 (2002).
[50] A. L. Piro and E. Pfahl, Astrophys. J. **658**, 1173 (2007).
[51] M. H. van Putten, A. Levinson, H. K. Lee, T. Regimbau, M. Punturo, and G. M. Harry, Phys. Rev. D **69**, 044007 (2004).
[52] S. Ando, F. Beacom, and H. Yüksel, Phys. Rev. Lett. **95**, 171101 (2005).
[53] M. Ando, T. Akutsu, T. Akutsu, K. Arai, Y. Aso, M. Fukushima, K. Hayama, N. Kanda, K. Kondo, N. Mio *et al.*, Classical Quantum Gravity **22**, S1283 (2005).
[54] B. Abbott *et al.* (LIGO Scientific Collaboration), Phys. Rev. D **69**, 102001 (2004).
[55] B. P. Abbott *et al.* (LIGO Scientific Collaboration), Classical Quantum Gravity **24**, 5343 (2007).
[56] B. P. Abbott *et al.* (LIGO Scientific Collaboration), Phys. Rev. D **80**, 102002 (2009).

[57] B. P. Abbott *et al.* (LIGO Scientific Collaboration), Phys. Rev. D **80**, 102001 (2009).
[58] J. Abadie *et al.* (LIGO Scientific Collaboration and Virgo Collaboration), Phys. Rev. D **81**, 102001 (2010).
[59] J. Abadie *et al.* (LIGO Scientific Collaboration and Virgo Collaboration), Phys. Rev. D **85**, 122007 (2012).
[60] M. H. P. M. van Putten, Astrophys. J. **819**, 169 (2016).
[61] P. J. Sutton, G. Jones, S. Chatterji, P. Kalmus, I. Leonor, S. Poprocki, J. Rollins, A. Searle, L. Stein, M. Tinto *et al.*, New J. Phys. **12**, 053034 (2010).
[62] B. P. Abbott *et al.* (LIGO Scientific Collaboration), Astrophys. J. **681**, 1419 (2008).
[63] B. Abbott *et al.* (LIGO Scientific Collaboration), Phys. Rev. D **77**, 062004 (2008).
[64] J. Abadie *et al.* (LIGO Scientific Collaboration and Virgo Collaboration), Astrophys. J. **715**, 1453 (2010).
[65] J. Abadie *et al.* (LIGO Scientific Collaboration), Astrophys. J. **755**, 2 (2012).
[66] J. Abadie *et al.* (LIGO Scientific Collaboration and Virgo Collaboration), Astrophys. J. **760**, 12 (2012).
[67] J. Aasi *et al.* (LIGO Scientific Collaboration and Virgo Collaboration), Phys. Rev. D **88**, 122004 (2013).
[68] J. Aasi *et al.* (LIGO Scientific Collaboration and Virgo Collaboration), Phys. Rev. D **89**, 122004 (2014).
[69] J. Aasi *et al.* (LIGO Scientific Collaboration and Virgo Collaboration), Phys. Rev. Lett. **113**, 011102 (2014).
[70] B. Abbott *et al.* (LIGO Scientific Collaboration), Phys. Rev. Lett. **101**, 211102 (2008).
[71] J. Abadie *et al.* (LIGO Scientific Collaboration), Astrophys. J. Lett. **734**, L35 (2011).
[72] J. Abadie *et al.* (LIGO Scientific Collaboration), Phys. Rev. D **83**, 042001 (2011).
[73] S. E. Gossan, P. Sutton, A. Stuver, M. Zanolin, K. Gill, and C. D. Ott, Phys. Rev. D **93**, 042002 (2016).
[74] K. Hayama, T. Kuroda, K. Kotake, and T. Takiwaki, Phys. Rev. D **92**, 122001 (2015).
[75] B. P. Abbott *et al.* (LIGO Scientific Collaboration), Rep. Prog. Phys. **72**, 076901 (2009).
[76] H. Grote (for the LIGO Scientific Collaboration), Classical Quantum Gravity **27**, 084003 (2010).
[77] T. Accadia, F. Acernese, M. Alshourbagy, P. Amico, F. Antonucci, S. Aoudia, N. Arnaud, C. Arnault, K. G. Arun, P. Astone *et al.*, J. Instrum. **7**, P03012 (2012).
[78] Harvard/CFA List of Supernovae, URLhttp://www.cfa.harvard.edu/iau/lists/Supernovae.html.
[79] M. H. P. M. van Putten, Astrophys. J. **819**, 169 (2016).
[80] G. Pagliaroli, F. Vissani, E. Coccia, and W. Fulgione, Phys. Rev. Lett. **103**, 031102 (2009).
[81] M. Ikeda *et al.* (Super-Kamiokande Collaboration), Astrophys. J. **669**, 519 (2007).
[82] I. Leonor, L. Cadonati, E. Coccia, S. D'Antonio, A. Di Credico, V. Fafone, R. Frey, W. Fulgione, E. Katsavounidis, C. D. Ott *et al.*, Classical Quantum Gravity **27**, 084019 (2010).
[83] K. Nakamura, S. Horiuchi, M. Tanaka, K. Hayama, T. Takiwaki, and K. Kotake, Mon. Not. R. Astron. Soc. **461**, 3296 (2016).
[84] S. J. Smartt, Annu. Rev. Astron. Astrophys. **47**, 63 (2009).
[85] M. C. Bersten, O. G. Benvenuto, K. Nomoto, M. Ergon, G. Folatelli, J. Sollerman, S. Benetti, M. T. Botticella, M. Fraser, R. Kotak *et al.*, Astrophys. J. **757**, 31 (2012).
[86] D. Kasen and S. E. Woosley, Astrophys. J. **703**, 2205 (2009).
[87] A. M. Soderberg, E. Berger, K. L. Page, P. Schady, J. Parrent, D. Pooley, X.-Y. Wang, E. O. Ofek, A. Cucchiara, A. Rau *et al.*, Nature (London) **453**, 469 (2008).
[88] S. Gezari, L. Dessart, S. Basa, D. C. Martin, J. D. Neill, S. E. Woosley, D. J. Hillier, G. Bazin, K. Forster, P. G. Friedman *et al.*, Astrophys. J. Lett. **683**, L131 (2008).
[89] D. F. Cowen, A. Franckowiak, and M. Kowalski, Astropart. Phys. **33**, 19 (2010).
[90] R. P. Kirshner and J. Kwan, Astrophys. J. **193**, 27 (1974).
[91] L. Dessart and D. J. Hillier, Astron. Astrophys. **439**, 671 (2005).
[92] D. Madison and W. Li, Central Bureau Electronic Telegrams **1034**, 1 (2007).
[93] A. V. Filippenko, W. D. Li, R. R. Treffers, and M. Modjaz, in *IAU Colloq. 183: Small Telescope Astronomy on Global Scales*, edited by B. Paczynski, W.-P. Chen, and C. Lemme (2001), Ast. Soc. Pac. Conf. Ser. Vol. 256, p. 121.
[94] R. M. Crockett, J. R. Maund, S. J. Smartt, S. Mattila, A. Pastorello, J. Smoker, A. W. Stephens, J. Fynbo, J. J. Eldridge, I. J. Danziger *et al.*, Astrophys. J. Lett. **672**, L99 (2008).
[95] P. A. Mazzali, I. Maurer, S. Valenti, R. Kotak, and D. Hunter, Mon. Not. R. Astron. Soc. **408**, 87 (2010).
[96] J. J. Eldridge, M. Fraser, S. J. Smartt, J. R. Maund, and R. M. Crockett, Mon. Not. R. Astron. Soc. **436**, 774 (2013).
[97] J. Chen, X. Wang, M. Ganeshalingam, J. M. Silverman, A. V. Filippenko, W. Li, R. Chornock, J. Li, and T. Steele, Astrophys. J. **790**, 120 (2014).
[98] B. P. Schmidt, R. P. Kirshner, R. G. Eastman, M. M. Phillips, N. B. Suntzeff, M. Hamuy, J. Maza, and R. Aviles, Astrophys. J. **432**, 42 (1994).
[99] N. A. Silbermann, P. Harding, B. F. Madore, R. C. Kennicutt, Jr., A. Saha, P. B. Stetson, W. L. Freedman, J. R. Mould, J. A. Graham, R. J. Hill *et al.*, Astrophys. J. **470**, 1 (1996).
[100] R. Chornock, A. V. Filippenko, W. Li, R. J. Foley, A. Stockton, E. C. Moran, J. Hodge, and K. Merriman, Central Bureau Electronic Telegrams **1298**, 1 (2008).
[101] R. Mostardi, W. Li, and A. V. Filippenko, Central Bureau Electronic Telegrams **1280**, 1 (2008).
[102] R. Arbour, Central Bureau Electronic Telegrams **1286**, 2 (2008).
[103] R. Chornock, A. V. Filippenko, W. Li, G. H. Marion, R. J. Foley, M. Modjaz, M. Rafelski, G. D. Becker, W. H. de Vries, P. Garnavich *et al.*, Astrophys. J. **739**, 41 (2011).
[104] R. M. Crockett, J. J. Eldridge, S. J. Smartt, A. Pastorello, A. Gal-Yam, D. B. Fox, D. C. Leonard, M. M. Kasliwal, S. Mattila, J. R. Maund *et al.*, Mon. Not. R. Astron. Soc. **391**, L5 (2008).
[105] G. Folatelli, M. C. Bersten, H. Kuncarayakti, O. G. Benvenuto, K. Maeda, and K. Nomoto, Astrophys. J. **811**, 147 (2015).

[106] A. Pastorello, M. M. Kasliwal, R. M. Crockett, S. Valenti, R. Arbour, K. Itagaki, S. Kaspi, A. Gal-Yam, S. J. Smartt, R. Griffith *et al.*, Mon. Not. R. Astron. Soc. **389**, 955 (2008).
[107] L. A. G. Monard, Central Bureau Electronic Telegrams **1315**, 1 (2008).
[108] N. Morrell and M. Stritzinger, Central Bureau Electronic Telegrams **1335**, 1 (2008).
[109] D. A. Howell, M. Sullivan, K. Perrett, T. J. Bronder, I. M. Hook, P. Astier, E. Aubourg, D. Balam, S. Basa, R. G. Carlberg *et al.*, Astrophys. J. **634**, 1190 (2005).
[110] L. Dessart (private communication).
[111] M. Hamuy, G. Pignata, J. Maza, A. Clocchiatti, J. Anderson, M. Bersten, G. Folatelli, F. Forster, C. Gutiérrez, J. Quinn *et al.*, Mem. Soc. Astron. Ital. **83**, 388 (2012).
[112] J. R. Maund, S. Mattila, E. Ramirez-Ruiz, and J. J. Eldridge, Mon. Not. R. Astron. Soc. **438**, 1577 (2014).
[113] S. D. Van Dyk, T. J. Davidge, N. Elias-Rosa, S. Taubenberger, W. Li, E. M. Levesque, S. Howerton, G. Pignata, N. Morrell, M. Hamuy *et al.*, Astron. J. **143**, 19 (2012).
[114] S. Mattila, S. J. Smartt, J. J. Eldridge, J. R. Maund, R. M. Crockett, and I. J. Danziger, Astrophys. J. Lett. **688**, L91 (2008).
[115] W. Li, S. D. van Dyk, A. V. Filippenko, R. J. Foley, G. Pignata, M. Hamuy, J. Moza, D. Reichart, K. Ivarsen, A. Crain *et al.*, Central Bureau Electronic Telegrams **1319**, 1 (2008).
[116] G. Pietrzyński, W. Gieren, M. Hamuy, G. Pignata, I. Soszyński, A. Udalski, A. Walker, P. Fouqué, F. Bresolin, R.-P. Kudritzki *et al.*, Astron. J. **140**, 1475 (2010).
[117] B. A. Jacobs, L. Rizzi, R. B. Tully, E. J. Shaya, D. I. Makarov, and L. Makarova, Astron. J. **138**, 332 (2009).
[118] M. G. Lee, W. L. Freedman, and B. F. Madore, Astrophys. J. **417**, 553 (1993).
[119] T. Griga, A. Marulla, A. Grenier, G. Sun, X. Gao, S. Lamotte Bailey, R. A. Koff, H. Mikuz, B. Dintinjana, J. M. Silverman *et al.*, Central Bureau Electronic Telegrams **2736**, 1 (2011).
[120] G. H. Marion, J. Vinko, R. P. Kirshner, R. J. Foley, P. Berlind, A. Bieryla, J. S. Bloom, M. L. Calkins, P. Challis, R. A. Chevalier *et al.*, Astrophys. J. **781**, 69 (2014).
[121] M. Ergon, J. Sollerman, M. Fraser, A. Pastorello, S. Taubenberger, N. Elias-Rosa, M. Bersten, A. Jerkstrand, S. Benetti, M. T. Botticella *et al.*, Astron. Astrophys. **562**, A17 (2014).
[122] A. Horesh, C. Stockdale, D. B. Fox, D. A. Frail, J. Carpenter, S. R. Kulkarni, E. O. Ofek, A. Gal-Yam, M. M. Kasliwal, I. Arcavi *et al.*, Mon. Not. R. Astron. Soc. **436**, 1258 (2013).
[123] Rochesterastronomy.org: SN 2011dh, URLhttp://www.rochesterastronomy.org/sn2011/sn2011dh.html.
[124] S. D. Van Dyk, W. Zheng, K. I. Clubb, A. V. Filippenko, S. B. Cenko, N. Smith, O. D. Fox, P. L. Kelly, I. Shivvers, and M. Ganeshalingam, Astrophys. J. Lett. **772**, L32 (2013).
[125] J. Vinkó, K. Takáts, T. Szalai, G. H. Marion, J. C. Wheeler, K. Sárneczky, P. M. Garnavich, J. Kelemen, P. Klagyivik, A. Pál *et al.*, Astron. Astrophys. **540**, A93 (2012).
[126] S. D. Van Dyk, W. Li, S. B. Cenko, M. M. Kasliwal, A. Horesh, E. O. Ofek, A. L. Kraus, J. M. Silverman, I. Arcavi, A. V. Filippenko *et al.*, Astrophys. J. Lett. **741**, L28 (2011).
[127] K. Sárneczky, N. Szalai, M. Kun, T. Szalai, K. Takáts, and J. Vinkó, Astronomer's Telegram **3406**, 1 (2011).
[128] J. J. Feldmeier, R. Ciardullo, and G. H. Jacoby, Astrophys. J. **479**, 231 (1997).
[129] J. L. Tonry, A. Dressler, J. P. Blakeslee, E. A. Ajhar, A. B. Fletcher, G. A. Luppino, M. R. Metzger, and C. B. Moore, Astrophys. J. **546**, 681 (2001).
[130] R. B. Tully, *Nearby Galaxies Catalog* (Cambridge University Press, Cambridge, UK, 1988).
[131] H. Grote, K. Danzmann, K. L. Dooley, R. Schnabel, J. Slutsky, and H. Vahlbruch, Phys. Rev. Lett. **110**, 181101 (2013).
[132] J. Aasi *et al.* (Virgo Collaboration and LIGO Scientific Collaboration), Classical Quantum Gravity **29**, 155002 (2012).
[133] J. Aasi *et al.* (LIGO Scientific Collaboration and Virgo Collaboration), Classical Quantum Gravity **32**, 115012 (2015).
[134] J. McIver, Classical Quantum Gravity **29**, 124010 (2012).
[135] M. Was, P. J. Sutton, G. Jones, and I. Leonor, Phys. Rev. D **86**, 022003 (2012).
[136] S. Klimenko, I. Yakushin, A. Mercer, and G. Mitselmakher, Classical Quantum Gravity **25**, 114029 (2008).
[137] C. Fryer and K. C. B. New, Living Rev. Relativ. **14**, 1 (2011).
[138] M. Drago, Ph. D. thesis, University of Padova (2011).
[139] S. Chatterji, A. Lazzarini, L. Stein, P. J. Sutton, A. Searle, and M. Tinto, Phys. Rev. D **74**, 082005 (2006).
[140] A. C. Searle, P. J. Sutton, M. Tinto, and G. Woan, Classical Quantum Gravity **25**, 114038 (2008).
[141] A. C. Searle, P. J. Sutton, and M. Tinto, Classical Quantum Gravity **26**, 155017 (2009).
[142] M. J. Szczepańczyk and C. D. Ott, LIGO Document Control Center (2015), URL https://dcc.ligo.org/LIGO-T1500586.
[143] C. D. Ott, LIGO Tech. Rep. No. LIGO-T1000553-v2 (2010).
[144] J. Abadie *et al.* (LIGO Scientific Collaboration and Virgo Collaboration), Phys. Rev. D **85**, 122007 (2012).
[145] E. Müller, Astron. Astrophys. **114**, 53 (1982).
[146] T. Zwerger and E. Müller, Astron. Astrophys. **320**, 209 (1997).
[147] H. Dimmelmeier, J. A. Font, and E. Müller, Astron. Astrophys. **393**, 523 (2002).
[148] K. Kotake, S. Yamada, and K. Sato, Phys. Rev. D **68**, 044023 (2003).
[149] C. D. Ott, A. Burrows, E. Livne, and R. Walder, Astrophys. J. **600**, 834 (2004).
[150] C. D. Ott, H. Dimmelmeier, A. Marek, H.-T. Janka, I. Hawke, B. Zink, and E. Schnetter, Phys. Rev. Lett. **98**, 261101 (2007).
[151] J. M. Lattimer and F. D. Swesty, Nucl. Phys. **A535**, 331 (1991).
[152] E. Müller and H.-T. Janka, Astron. Astrophys. **317**, 140 (1997).
[153] E. Müller, M. Rampp, R. Buras, H.-T. Janka, and D. H. Shoemaker, Astrophys. J. **603**, 221 (2004).

[154] K. Kotake, N. Ohnishi, and S. Yamada, Astrophys. J. **655**, 406 (2007).
[155] J. W. Murphy, C. D. Ott, and A. Burrows, Astrophys. J. **707**, 1173 (2009).
[156] K. Kotake, W. Iwakami, N. Ohnishi, and S. Yamada, Astrophys. J. Lett. **697**, L133 (2009).
[157] A. Marek, H.-T. Janka, and E. Müller, Astron. Astrophys. **496**, 475 (2009).
[158] S. Scheidegger, R. Käppeli, S. C. Whitehouse, T. Fischer, and M. Liebendörfer, Astron. Astrophys. **514**, A51 (2010).
[159] T. Takiwaki, K. Kotake, and Y. Suwa, Mon. Not. R. Astron. Soc. Lett. **461**, L112 (2016).
[160] S. E. Gossan, P. Sutton, A. Stuver, M. Zanolin, K. Gill, and C. D. Ott, Phys. Rev. D **93**, 042002 (2016).
[161] S. Scheidegger, S. C. Whitehouse, R. Käppeli, and M. Liebendörfer, Classical Quantum Gravity **27**, 114101 (2010).
[162] A. Burrows, E. Livne, L. Dessart, C. D. Ott, and J. Murphy, Astrophys. J. **640**, 878 (2006).
[163] A. Burrows, E. Livne, L. Dessart, C. D. Ott, and J. Murphy, Astrophys. J. **655**, 416 (2007).
[164] A. Marek and H.-T. Janka, Astrophys. J. **694**, 664 (2009).
[165] D. Lai and S. L. Shapiro, Astrophys. J. **442**, 259 (1995).
[166] J. D. Brown, AIP Conf. Proc. **575** (2001), p. 234.
[167] M. Shibata and Y.-I. Sekiguchi, Phys. Rev. D **71**, 024014 (2005).
[168] M. Rampp, E. Müller, and M. Ruffert, Astron. Astrophys. **332**, 969 (1998).
[169] C. D. Ott, S. Ou, J. E. Tohline, and A. Burrows, Astrophys. J. **625**, L119 (2005).
[170] L. Santamaria and C. D. Ott, LIGO Tech. Rep. No. LIGO-T1100093-v2.
[171] M. Paterno, Fermilab Tech. Rep. No. FERMILAB-TM-2286-CD (2004).
[172] J. Abadie *et al.* (LIGO Scientific Collaboration and Virgo Collaboration), Nucl. Instrum. Methods Phys. Res., Sect. A **624**, 223 (2010).
[173] F. Marion, B. Mours, and L. Rolland, Tech. Rep. No. VIR-0078A-08 (2010).
[174] P. J. Sutton, arXiv:1304.0210.
[175] J. M. Lattimer and M. Prakash, Astrophys. J. **550**, 426 (2001).
[176] F. Vissani, J. Phys. G **42**, 013001 (2015).
[177] P. Kalmus, M. Zanolin, and S. Klimenko, LIGO Document Control Center (2013), URL https://dcc.ligo.org/LIGO-P1300018.
[178] B. P. Abbott, R. Abbott, T. D. Abbott, M. R. Abernathy, F. Acernese, K. Ackley, C. Adams, T. Adams, P. Addesso, R. X. Adhikari *et al.* (LIGO Scientific Collaboration and Virgo Collaboration), Living Rev. Relativ. **19** (2016).

B. P. Abbott,[1] R. Abbott,[1] T. D. Abbott,[2] M. R. Abernathy,[1] F. Acernese,[3,4] K. Ackley,[5] C. Adams,[6] T. Adams,[7] P. Addesso,[8] R. X. Adhikari,[1] V. B. Adya,[9] C. Affeldt,[9] M. Agathos,[10] K. Agatsuma,[10] N. Aggarwal,[11] O. D. Aguiar,[12] L. Aiello,[13,14] A. Ain,[15] P. Ajith,[16] B. Allen,[9,17,18] A. Allocca,[19,20] P. A. Altin,[21] S. B. Anderson,[1] W. G. Anderson,[17] K. Arai,[1] M. C. Araya,[1] C. C. Arceneaux,[22] J. S. Areeda,[23] N. Arnaud,[24] K. G. Arun,[25] S. Ascenzi,[26,14] G. Ashton,[27] M. Ast,[28] S. M. Aston,[6] P. Astone,[29] P. Aufmuth,[18] C. Aulbert,[9] S. Babak,[30] P. Bacon,[31] M. K. M. Bader,[10] P. T. Baker,[32] F. Baldaccini,[33,34] G. Ballardin,[35] S. W. Ballmer,[36] J. C. Barayoga,[1] S. E. Barclay,[37] B. C. Barish,[1] D. Barker,[38] F. Barone,[3,4] B. Barr,[37] L. Barsotti,[11] M. Barsuglia,[31] D. Barta,[39] J. Bartlett,[38] I. Bartos,[40] R. Bassiri,[41] A. Basti,[19,20] J. C. Batch,[38] C. Baune,[9] V. Bavigadda,[35] M. Bazzan,[42,43] B. Behnke,[30] M. Bejger,[44] A. S. Bell,[37] C. J. Bell,[37] B. K. Berger,[1] J. Bergman,[38] G. Bergmann,[9] C. P. L. Berry,[45] D. Bersanetti,[46,47] A. Bertolini,[10] J. Betzwieser,[6] S. Bhagwat,[36] R. Bhandare,[48] I. A. Bilenko,[49] G. Billingsley,[1] J. Birch,[6] R. Birney,[50] S. Biscans,[11] A. Bisht,[9,18] M. Bitossi,[35] C. Biwer,[36] M. A. Bizouard,[24] J. K. Blackburn,[1] C. D. Blair,[51] D. G. Blair,[51] R. M. Blair,[38] S. Bloemen,[52] O. Bock,[9] T. P. Bodiya,[11] M. Boer,[53] G. Bogaert,[53] C. Bogan,[9] A. Bohe,[30] P. Bojtos,[54] C. Bond,[45] F. Bondu,[55] R. Bonnand,[7] B. A. Boom,[10] R. Bork,[1] V. Boschi,[19,20] S. Bose,[56,15] Y. Bouffanais,[31] A. Bozzi,[35] C. Bradaschia,[20] P. R. Brady,[17] V. B. Braginsky,[49] M. Branchesi,[57,58] J. E. Brau,[59] T. Briant,[60] A. Brillet,[53] M. Brinkmann,[9] V. Brisson,[24] P. Brockill,[17] A. F. Brooks,[1] D. A. Brown,[36] D. D. Brown,[45] N. M. Brown,[11] C. C. Buchanan,[2] A. Buikema,[11] T. Bulik,[61] H. J. Bulten,[62,10] A. Buonanno,[30,63] D. Buskulic,[7] C. Buy,[31] R. L. Byer,[41] L. Cadonati,[64] G. Cagnoli,[65,66] C. Cahillane,[1] J. Calderón Bustillo,[67,64] T. Callister,[1] E. Calloni,[68,4] J. B. Camp,[69] K. C. Cannon,[70] J. Cao,[71] C. D. Capano,[9] E. Capocasa,[31] F. Carbognani,[35] S. Caride,[72] J. Casanueva Diaz,[24] C. Casentini,[26,14] S. Caudill,[17] M. Cavaglià,[22] F. Cavalier,[24] R. Cavalieri,[35] G. Cella,[20] C. B. Cepeda,[1] L. Cerboni Baiardi,[57,58] G. Cerretani,[19,20] E. Cesarini,[26,14] R. Chakraborty,[1] T. Chalermsongsak,[1] S. J. Chamberlin,[17] M. Chan,[37] S. Chao,[73] P. Charlton,[74] E. Chassande-Mottin,[31] H. Y. Chen,[75] Y. Chen,[76] C. Cheng,[73] A. Chincarini,[47] A. Chiummo,[35] H. S. Cho,[77] M. Cho,[63] J. H. Chow,[21] N. Christensen,[78] Q. Chu,[51] S. Chua,[60] S. Chung,[51] G. Ciani,[5] F. Clara,[38] J. A. Clark,[64] F. Cleva,[53] E. Coccia,[26,13] P.-F. Cohadon,[60] A. Colla,[79,29] C. G. Collette,[80] L. Cominsky,[81] M. Constancio Jr.,[12] A. Conte,[79,29] L. Conti,[43] D. Cook,[38] T. R. Corbitt,[2] N. Cornish,[32] A. Corpuz,[97] A. Corsi,[82] S. Cortese,[35] C. A. Costa,[12] M. W. Coughlin,[78] S. B. Coughlin,[83] J.-P. Coulon,[53] S. T. Countryman,[40] P. Couvares,[1] D. M. Coward,[51]

M. J. Cowart,[6] D. C. Coyne,[1] R. Coyne,[82] K. Craig,[37] J. D. E. Creighton,[17] J. Cripe,[2] S. G. Crowder,[84] A. Cumming,[37] L. Cunningham,[37] E. Cuoco,[35] T. Dal Canton,[9] S. L. Danilishin,[37] S. D'Antonio,[14] K. Danzmann,[18,9] N. S. Darman,[85] V. Dattilo,[35] I. Dave,[48] H. P. Daveloza,[86] M. Davier,[24] G. S. Davies,[37] E. J. Daw,[87] R. Day,[35] D. DeBra,[41] G. Debreczeni,[39] J. Degallaix,[65] M. De Laurentis,[68,4] S. Deléglise,[60] W. Del Pozzo,[45] T. Denker,[9,18] T. Dent,[9] V. Dergachev,[1] R. De Rosa,[68,4] R. T. DeRosa,[6] R. DeSalvo,[8] S. Dhurandhar,[15] M. C. Díaz,[86] L. Di Fiore,[4] M. Di Giovanni,[88,89] T. Di Girolamo,[68,4] A. Di Lieto,[19,20] S. Di Pace,[79,29] I. Di Palma,[30,9] A. Di Virgilio,[20] G. Dojcinoski,[90] V. Dolique,[65] F. Donovan,[11] K. L. Dooley,[22] S. Doravari,[6] R. Douglas,[37] T. P. Downes,[17] M. Drago,[9] R. W. P. Drever,[1] J. C. Driggers,[38] Z. Du,[71] M. Ducrot,[7] S. E. Dwyer,[38] T. B. Edo,[87] M. C. Edwards,[78] A. Effler,[6] H.-B. Eggenstein,[9] P. Ehrens,[1] J. Eichholz,[5] S. S. Eikenberry,[5] W. Engels,[76] R. C. Essick,[11] T. Etzel,[1] M. Evans,[11] T. M. Evans,[6] R. Everett,[91] M. Factourovich,[40] V. Fafone,[26,14] H. Fair,[36] S. Fairhurst,[83] X. Fan,[71] Q. Fang,[51] S. Farinon,[47] B. Farr,[75] W. M. Farr,[45] M. Favata,[90] M. Fays,[83] H. Fehrmann,[9] M. M. Fejer,[41] I. Ferrante,[19,20] E. C. Ferreira,[12] F. Ferrini,[35] F. Fidecaro,[19,20] I. Fiori,[35] D. Fiorucci,[31] R. P. Fisher,[36] R. Flaminio,[65,92] M. Fletcher,[37] J.-D. Fournier,[53] S. Frasca,[79,29] F. Frasconi,[20] Z. Frei,[54] A. Freise,[45] R. Frey,[59] V. Frey,[24] T. T. Fricke,[9] P. Fritschel,[11] V. V. Frolov,[6] P. Fulda,[5] M. Fyffe,[6] H. A. G. Gabbard,[22] J. R. Gair,[93] L. Gammaitoni,[33] S. G. Gaonkar,[15] F. Garufi,[68,4] G. Gaur,[94,95] N. Gehrels,[69] G. Gemme,[47] E. Genin,[35] A. Gennai,[20] J. George,[48] L. Gergely,[96] V. Germain,[7] Archisman Ghosh,[16] S. Ghosh,[52,10] J. A. Giaime,[2,6] K. D. Giardina,[6] A. Giazotto,[20] K. Gill,[97] A. Glaefke,[37] E. Goetz,[72] R. Goetz,[5] L. Gondan,[54] G. González,[2] J. M. Gonzalez Castro,[19,20] A. Gopakumar,[98] N. A. Gordon,[37] M. L. Gorodetsky,[49] S. E. Gossan,[1] M. Gosselin,[35] R. Gouaty,[7] A. Grado,[99,4] C. Graef,[37] P. B. Graff,[69,63] M. Granata,[65] A. Grant,[37] S. Gras,[11] C. Gray,[38] G. Greco,[57,58] A. C. Green,[45] P. Groot,[52] H. Grote,[9] S. Grunewald,[30] G. M. Guidi,[57,58] X. Guo,[71] A. Gupta,[15] M. K. Gupta,[95] K. E. Gushwa,[1] E. K. Gustafson,[1] R. Gustafson,[72] J. J. Hacker,[23] B. R. Hall,[56] E. D. Hall,[1] G. Hammond,[37] M. Haney,[98] M. M. Hanke,[9] J. Hanks,[38] C. Hanna,[91] M. D. Hannam,[83] J. Hanson,[6] T. Hardwick,[2] J. Harms,[57,58] G. M. Harry,[100] I. W. Harry,[30] M. J. Hart,[37] M. T. Hartman,[5] C.-J. Haster,[45] K. Haughian,[37] A. Heidmann,[60] M. C. Heintze,[5,6] H. Heitmann,[53] P. Hello,[24] G. Hemming,[35] M. Hendry,[37] I. S. Heng,[37] J. Hennig,[37] A. W. Heptonstall,[1] M. Heurs,[9,18] S. Hild,[37] D. Hoak,[101,35] K. A. Hodge,[1] D. Hofman,[65] S. E. Hollitt,[102] K. Holt,[6] D. E. Holz,[75] P. Hopkins,[83] D. J. Hosken,[102] J. Hough,[37] E. A. Houston,[37] E. J. Howell,[51] Y. M. Hu,[37] S. Huang,[73] E. A. Huerta,[103] D. Huet,[24] B. Hughey,[97] S. Husa,[67] S. H. Huttner,[37] T. Huynh-Dinh,[6] A. Idrisy,[91] N. Indik,[9] D. R. Ingram,[38] R. Inta,[82] H. N. Isa,[37] J.-M. Isac,[60] M. Isi,[1] G. Islas,[23] T. Isogai,[11] B. R. Iyer,[16] K. Izumi,[38] T. Jacqmin,[60] H. Jang,[77] K. Jani,[64] P. Jaranowski,[104] S. Jawahar,[105] F. Jiménez-Forteza,[67] W. W. Johnson,[2] D. I. Jones,[27] R. Jones,[37] R. J. G. Jonker,[10] L. Ju,[51] K. Haris,[106] C. V. Kalaghatgi,[25] P. Kalmus,[1] V. Kalogera,[107] I. Kamaretsos,[83] S. Kandhasamy,[22] G. Kang,[77] J. B. Kanner,[1] S. Karki,[59] M. Kasprzack,[2,35] E. Katsavounidis,[11] W. Katzman,[6] S. Kaufer,[18] T. Kaur,[51] K. Kawabe,[38] F. Kawazoe,[9] F. Kéfélian,[53] M. S. Kehl,[70] D. Keitel,[9] D. B. Kelley,[36] W. Kells,[1] R. Kennedy,[87] J. S. Key,[86] A. Khalaidovski,[9] F. Y. Khalili,[49] I. Khan,[13] S. Khan,[83] Z. Khan,[95] E. A. Khazanov,[108] N. Kijbunchoo,[38] Chunglee Kim,[77] J. Kim,[109] K. Kim,[110] Nam-Gyu Kim,[77] Namjun Kim,[41] Y.-M. Kim,[109] E. J. King,[102] P. J. King,[38] D. L. Kinzel,[6] J. S. Kissel,[38] L. Kleybolte,[28] S. Klimenko,[5] S. M. Koehlenbeck,[9] K. Kokeyama,[2] S. Koley,[10] V. Kondrashov,[1] A. Kontos,[11] M. Korobko,[28] W. Z. Korth,[1] I. Kowalska,[61] D. B. Kozak,[1] V. Kringel,[9] B. Krishnan,[9] A. Królak,[111,112] C. Krueger,[18] G. Kuehn,[9] P. Kumar,[70] L. Kuo,[73] A. Kutynia,[111] B. D. Lackey,[36] M. Landry,[38] J. Lange,[113] B. Lantz,[41] P. D. Lasky,[114] A. Lazzarini,[1] C. Lazzaro,[64,43] P. Leaci,[79,29] S. Leavey,[37] E. O. Lebigot,[31,71] C. H. Lee,[109] H. K. Lee,[110] H. M. Lee,[115] K. Lee,[37] A. Lenon,[36] M. Leonardi,[88,89] J. R. Leong,[9] N. Leroy,[24] N. Letendre,[7] Y. Levin,[114] B. M. Levine,[38] T. G. F. Li,[1] A. Libson,[11] T. B. Littenberg,[116] N. A. Lockerbie,[105] K. Loew,[97] J. Logue,[37] A. L. Lombardi,[101] J. E. Lord,[36] M. Lorenzini,[13,14] V. Loriette,[117] M. Lormand,[6] G. Losurdo,[58] J. D. Lough,[9,18] H. Lück,[18,9] A. P. Lundgren,[9] J. Luo,[78] R. Lynch,[11] Y. Ma,[51] T. MacDonald,[41] B. Machenschalk,[9] M. MacInnis,[11] D. M. Macleod,[2] F. Magaña-Sandoval,[36] R. M. Magee,[56] M. Mageswaran,[1] E. Majorana,[29] I. Maksimovic,[117] V. Malvezzi,[26,14] N. Man,[53] I. Mandel,[45] V. Mandic,[84] V. Mangano,[37] G. L. Mansell,[21] M. Manske,[17] M. Mantovani,[35] F. Marchesoni,[118,34] F. Marion,[7] S. Márka,[40] Z. Márka,[40] A. S. Markosyan,[41] E. Maros,[1] F. Martelli,[57,58] L. Martellini,[53] I. W. Martin,[37] R. M. Martin,[5] D. V. Martynov,[1] J. N. Marx,[1] K. Mason,[11] A. Masserot,[7] T. J. Massinger,[36] M. Masso-Reid,[37] S. Mastrogiovanni,[79,29] F. Matichard,[11] L. Matone,[40] N. Mavalvala,[11] N. Mazumder,[56] G. Mazzolo,[9] R. McCarthy,[38] D. E. McClelland,[21] S. McCormick,[6] S. C. McGuire,[119] G. McIntyre,[1] J. McIver,[101] D. J. McManus,[21] S. T. McWilliams,[103] D. Meacher,[53] G. D. Meadors,[30,9] J. Meidam,[10] A. Melatos,[85] G. Mendell,[38] D. Mendoza-Gandara,[9] R. A. Mercer,[17] E. L. Merilh,[38] M. Merzougui,[53] S. Meshkov,[1] C. Messenger,[37] C. Messick,[91] R. Metzdorff,[60] P. M. Meyers,[84] F. Mezzani,[29,79] H. Miao,[45] C. Michel,[65] H. Middleton,[45] E. E. Mikhailov,[120] L. Milano,[68,4] A. L. Miller,[5,79,29] J. Miller,[11] M. Millhouse,[32] Y. Minenkov,[14] J. Ming,[30,9] S. Mirshekari,[121] C. Mishra,[16]

S. Mitra,[15] V. P. Mitrofanov,[49] G. Mitselmakher,[5] R. Mittleman,[11] A. Moggi,[20] M. Mohan,[35] S. R. P. Mohapatra,[11] M. Montani,[57,58] B. C. Moore,[90] C. J. Moore,[122] D. Moraru,[38] G. Moreno,[38] S. R. Morriss,[86] K. Mossavi,[9] B. Mours,[7] C. M. Mow-Lowry,[45] C. L. Mueller,[5] G. Mueller,[5] A. W. Muir,[83] Arunava Mukherjee,[16] D. Mukherjee,[17] S. Mukherjee,[86] K. N. Mukund,[15] A. Mullavey,[6] J. Munch,[102] D. J. Murphy,[40] P. G. Murray,[37] A. Mytidis,[5] I. Nardecchia,[26,14] L. Naticchioni,[79,29] R. K. Nayak,[123] V. Necula,[5] K. Nedkova,[101] G. Nelemans,[52,10] M. Neri,[46,47] A. Neunzert,[72] G. Newton,[37] T. T. Nguyen,[21] A. B. Nielsen,[9] S. Nissanke,[52,10] A. Nitz,[9] F. Nocera,[35] D. Nolting,[6] M. E. N. Normandin,[86] L. K. Nuttall,[36] J. Oberling,[38] E. Ochsner,[17] J. O'Dell,[124] E. Oelker,[11] G. H. Ogin,[125] J. J. Oh,[126] S. H. Oh,[126] F. Ohme,[83] M. Oliver,[67] P. Oppermann,[9] Richard J. Oram,[6] B. O'Reilly,[6] R. O'Shaughnessy,[113] C. D. Ott,[76] D. J. Ottaway,[102] R. S. Ottens,[5] H. Overmier,[6] B. J. Owen,[82] A. Pai,[106] S. A. Pai,[48] J. R. Palamos,[59] O. Palashov,[108] C. Palomba,[29] A. Pal-Singh,[28] H. Pan,[73] C. Pankow,[17,107] F. Pannarale,[83] B. C. Pant,[48] F. Paoletti,[35,20] A. Paoli,[35] M. A. Papa,[30,17,9] H. R. Paris,[41] W. Parker,[6] D. Pascucci,[37] A. Pasqualetti,[35] R. Passaquieti,[19,20] D. Passuello,[20] B. Patricelli,[19,20] Z. Patrick,[41] B. L. Pearlstone,[37] M. Pedraza,[1] R. Pedurand,[65,127] L. Pekowsky,[36] A. Pele,[6] S. Penn,[128] R. Pereira,[40] A. Perreca,[1] M. Phelps,[37] O. J. Piccinni,[79,29] M. Pichot,[53] F. Piergiovanni,[57,58] V. Pierro,[8] G. Pillant,[35] L. Pinard,[65] I. M. Pinto,[8] M. Pitkin,[37] R. Poggiani,[19,20] P. Popolizio,[35] A. Post,[9] J. Powell,[37] J. Prasad,[15] V. Predoi,[83] S. S. Premachandra,[114] T. Prestegard,[84] L. R. Price,[1] M. Prijatelj,[35] M. Principe,[8] S. Privitera,[30] R. Prix,[9] G. A. Prodi,[88,89] L. Prokhorov,[49] O. Puncken,[9] M. Punturo,[34] P. Puppo,[29] M. Pürrer,[83] H. Qi,[17] J. Qin,[51] V. Quetschke,[86] E. A. Quintero,[1] R. Quitzow-James,[59] F. J. Raab,[38] D. S. Rabeling,[21] H. Radkins,[38] P. Raffai,[54] S. Raja,[48] M. Rakhmanov,[86] P. Rapagnani,[79,29] V. Raymond,[30] M. Razzano,[19,20] V. Re,[26] J. Read,[23] C. M. Reed,[38] T. Regimbau,[53] L. Rei,[47] S. Reid,[50] D. H. Reitze,[1,5] H. Rew,[120] F. Ricci,[79,29] K. Riles,[72] N. A. Robertson,[1,37] R. Robie,[37] F. Robinet,[24] A. Rocchi,[14] L. Rolland,[7] J. G. Rollins,[1] V. J. Roma,[59] J. D. Romano,[86] R. Romano,[3,4] G. Romanov,[120] J. H. Romie,[6] D. Rosińska,[129,44] S. Rowan,[37] A. Rüdiger,[9] P. Ruggi,[35] K. Ryan,[38] S. Sachdev,[1] T. Sadecki,[38] L. Sadeghian,[17] L. Salconi,[35] M. Saleem,[106] F. Salemi,[9] A. Samajdar,[123] L. Sammut,[85,114] E. J. Sanchez,[1] V. Sandberg,[38] B. Sandeen,[107] J. R. Sanders,[72] L. Santamaria,[1] B. Sassolas,[65] B. S. Sathyaprakash,[83] P. R. Saulson,[36] O. E. S. Sauter,[72] R. L. Savage,[38] A. Sawadsky,[18] P. Schale,[59] R. Schilling,[9,†] J. Schmidt,[9] P. Schmidt,[1,76] R. Schnabel,[28] R. M. S. Schofield,[59] A. Schönbeck,[28] E. Schreiber,[9] D. Schuette,[9,18] B. F. Schutz,[83] J. Scott,[37] S. M. Scott,[21] D. Sellers,[6] D. Sentenac,[35] V. Sequino,[26,14] A. Sergeev,[108] G. Serna,[23] Y. Setyawati,[52,10] A. Sevigny,[38] D. A. Shaddock,[21] M. S. Shahriar,[107] M. Shaltev,[9] Z. Shao,[1] B. Shapiro,[41] P. Shawhan,[63] A. Sheperd,[17] D. H. Shoemaker,[11] D. M. Shoemaker,[64] K. Siellez,[53] X. Siemens,[17] M. Sieniawska,[44] D. Sigg,[38] A. D. Silva,[12] D. Simakov,[9] A. Singer,[1] L. P. Singer,[69] A. Singh,[30,9] R. Singh,[2] A. Singhal,[13] A. M. Sintes,[67] B. J. J. Slagmolen,[21] J. R. Smith,[23] N. D. Smith,[1] R. J. E. Smith,[1] E. J. Son,[126] B. Sorazu,[37] F. Sorrentino,[47] T. Souradeep,[15] A. K. Srivastava,[95] A. Staley,[40] M. Steinke,[9] J. Steinlechner,[37] S. Steinlechner,[37] D. Steinmeyer,[9,18] B. C. Stephens,[17] R. Stone,[86] K. A. Strain,[37] N. Straniero,[65] G. Stratta,[57,58] N. A. Strauss,[78] S. Strigin,[49] R. Sturani,[121] A. L. Stuver,[6] T. Z. Summerscales,[130] L. Sun,[85] P. J. Sutton,[83] B. L. Swinkels,[35] M. J. Szczepańczyk,[97] M. Tacca,[31] D. Talukder,[59] D. B. Tanner,[5] M. Tápai,[96] S. P. Tarabrin,[9] A. Taracchini,[30] R. Taylor,[1] T. Theeg,[9] M. P. Thirugnanasambandam,[1] E. G. Thomas,[45] M. Thomas,[6] P. Thomas,[38] K. A. Thorne,[6] K. S. Thorne,[76] E. Thrane,[114] S. Tiwari,[13,89] V. Tiwari,[83] K. V. Tokmakov,[105] C. Tomlinson,[87] M. Tonelli,[19,20] C. V. Torres,[86,†] C. I. Torrie,[1] D. Töyrä,[45] F. Travasso,[33,34] G. Traylor,[6] D. Trifirò,[22] M. C. Tringali,[88,89] L. Trozzo,[131,20] M. Tse,[11] M. Turconi,[53] D. Tuyenbayev,[86] D. Ugolini,[132] C. S. Unnikrishnan,[98] A. L. Urban,[17] S. A. Usman,[36] H. Vahlbruch,[18] G. Vajente,[1] G. Valdes,[86] N. van Bakel,[10] M. van Beuzekom,[10] J. F. J. van den Brand,[62,10] C. Van Den Broeck,[10] D. C. Vander-Hyde,[36,23] L. van der Schaaf,[10] J. V. van Heijningen,[10] A. A. van Veggel,[37] M. Vardaro,[42,43] S. Vass,[1] M. Vasúth,[39] R. Vaulin,[11] A. Vecchio,[45] G. Vedovato,[43] J. Veitch,[45] P. J. Veitch,[102] K. Venkateswara,[133] D. Verkindt,[7] F. Vetrano,[57,58] A. Viceré,[57,58] S. Vinciguerra,[45] D. J. Vine,[50] J.-Y. Vinet,[53] S. Vitale,[11] T. Vo,[36] H. Vocca,[33,34] C. Vorvick,[38] D. V. Voss,[5] W. D. Vousden,[45] S. P. Vyatchanin,[49] A. R. Wade,[21] L. E. Wade,[134] M. Wade,[134] M. Walker,[2] L. Wallace,[1] S. Walsh,[17] G. Wang,[13,58] H. Wang,[45] M. Wang,[45] X. Wang,[71] Y. Wang,[51] R. L. Ward,[21] J. Warner,[38] M. Was,[7] B. Weaver,[38] L.-W. Wei,[53] M. Weinert,[9] A. J. Weinstein,[1] R. Weiss,[11] T. Welborn,[6] L. Wen,[51] P. Weßels,[9] T. Westphal,[9] K. Wette,[9] J. T. Whelan,[113,9] S. E. Whitcomb,[1] D. J. White,[87] B. F. Whiting,[5] R. D. Williams,[1] A. R. Williamson,[83] J. L. Willis,[135] B. Willke,[18,9] M. H. Wimmer,[9,18] W. Winkler,[9] C. C. Wipf,[1] H. Wittel,[9,18] G. Woan,[37] J. Worden,[38] J. L. Wright,[37] G. Wu,[6] J. Yablon,[107] W. Yam,[11] H. Yamamoto,[1] C. C. Yancey,[63] M. J. Yap,[21] H. Yu,[11] M. Yvert,[7] A. Zadrożny,[111] L. Zangrando,[43] M. Zanolin,[97] J.-P. Zendri,[43] M. Zevin,[107] F. Zhang,[11] L. Zhang,[1] M. Zhang,[120] Y. Zhang,[113] C. Zhao,[51] M. Zhou,[107] Z. Zhou,[107] X. J. Zhu,[51] M. E. Zucker,[1,11] S. E. Zuraw,[101] and J. Zweizig[1]

(LIGO Scientific Collaboration and Virgo Collaboration)

*

[1]LIGO, California Institute of Technology, Pasadena, California 91125, USA
[2]Louisiana State University, Baton Rouge, Louisiana 70803, USA
[3]Università di Salerno, Fisciano, I-84084 Salerno, Italy
[4]INFN, Sezione di Napoli, Complesso Universitario di Monte S.Angelo, I-80126 Napoli, Italy
[5]University of Florida, Gainesville, Florida 32611, USA
[6]LIGO Livingston Observatory, Livingston, Louisiana 70754, USA
[7]Laboratoire d'Annecy-le-Vieux de Physique des Particules (LAPP), Université Savoie Mont Blanc, CNRS/IN2P3, F-74941 Annecy-le-Vieux, France
[8]University of Sannio at Benevento, I-82100 Benevento, Italy and INFN, Sezione di Napoli, I-80100 Napoli, Italy
[9]Albert-Einstein-Institut, Max-Planck-Institut für Gravitationsphysik, D-30167 Hannover, Germany
[10]Nikhef, Science Park, 1098 XG Amsterdam, Netherlands
[11]LIGO, Massachusetts Institute of Technology, Cambridge, Massachusetts 02139, USA
[12]Instituto Nacional de Pesquisas Espaciais, 12227-010 São José dos Campos, São Paulo, Brazil
[13]INFN, Gran Sasso Science Institute, I-67100 L'Aquila, Italy
[14]INFN, Sezione di Roma Tor Vergata, I-00133 Roma, Italy
[15]Inter-University Centre for Astronomy and Astrophysics, Pune 411007, India
[16]International Centre for Theoretical Sciences, Tata Institute of Fundamental Research, Bangalore 560012, India
[17]University of Wisconsin-Milwaukee, Milwaukee, Wisconsin 53201, USA
[18]Leibniz Universität Hannover, D-30167 Hannover, Germany
[19]Università di Pisa, I-56127 Pisa, Italy
[20]INFN, Sezione di Pisa, I-56127 Pisa, Italy
[21]Australian National University, Canberra, Australian Capital Territory 0200, Australia
[22]The University of Mississippi, University, Mississippi 38677, USA
[23]California State University Fullerton, Fullerton, California 92831, USA
[24]LAL, Univ. Paris-Sud, CNRS/IN2P3, Université Paris-Saclay, 91400 Orsay, France
[25]Chennai Mathematical Institute, Chennai 603103, India
[26]Università di Roma Tor Vergata, I-00133 Roma, Italy
[27]University of Southampton, Southampton SO17 1BJ, United Kingdom
[28]Universität Hamburg, D-22761 Hamburg, Germany
[29]INFN, Sezione di Roma, I-00185 Roma, Italy
[30]Albert-Einstein-Institut, Max-Planck-Institut für Gravitationsphysik, D-14476 Potsdam-Golm, Germany
[31]APC, AstroParticule et Cosmologie, Université Paris Diderot, CNRS/IN2P3, CEA/Irfu, Observatoire de Paris, Sorbonne Paris Cité, F-75205 Paris Cedex 13, France
[32]Montana State University, Bozeman, Montana 59717, USA
[33]Università di Perugia, I-06123 Perugia, Italy
[34]INFN, Sezione di Perugia, I-06123 Perugia, Italy
[35]European Gravitational Observatory (EGO), I-56021 Cascina, Pisa, Italy
[36]Syracuse University, Syracuse, New York 13244, USA
[37]SUPA, University of Glasgow, Glasgow G12 8QQ, United Kingdom
[38]LIGO Hanford Observatory, Richland, Washington 99352, USA
[39]Wigner RCP, RMKI, H-1121 Budapest, Konkoly Thege Miklós út 29-33, Hungary
[40]Columbia University, New York, New York 10027, USA
[41]Stanford University, Stanford, California 94305, USA
[42]Università di Padova, Dipartimento di Fisica e Astronomia, I-35131 Padova, Italy
[43]INFN, Sezione di Padova, I-35131 Padova, Italy
[44]CAMK-PAN, 00-716 Warsaw, Poland
[45]University of Birmingham, Birmingham B15 2TT, United Kingdom
[46]Università degli Studi di Genova, I-16146 Genova, Italy
[47]INFN, Sezione di Genova, I-16146 Genova, Italy
[48]RRCAT, Indore Madhya Pradesh 452013, India
[49]Faculty of Physics, Lomonosov Moscow State University, Moscow 119991, Russia
[50]SUPA, University of the West of Scotland, Paisley PA1 2BE, United Kingdom
[51]University of Western Australia, Crawley, Western Australia 6009, Australia
[52]Department of Astrophysics/IMAPP, Radboud University Nijmegen, P.O. Box 9010, 6500 GL Nijmegen, Netherlands

[53]*Artemis, Université Côte d'Azur, CNRS, Observatoire Côte d'Azur, CS 34229, Nice cedex 4, France*
[54]*MTA Eötvös University, "Lendulet" Astrophysics Research Group, Budapest 1117, Hungary*
[55]*Institut de Physique de Rennes, CNRS, Université de Rennes 1, F-35042 Rennes, France*
[56]*Washington State University, Pullman, Washington 99164, USA*
[57]*Università degli Studi di Urbino "Carlo Bo," I-61029 Urbino, Italy*
[58]*INFN, Sezione di Firenze, I-50019 Sesto Fiorentino, Firenze, Italy*
[59]*University of Oregon, Eugene, Oregon 97403, USA*
[60]*Laboratoire Kastler Brossel, UPMC-Sorbonne Universités, CNRS, ENS-PSL Research University, Collège de France, F-75005 Paris, France*
[61]*Astronomical Observatory Warsaw University, 00-478 Warsaw, Poland*
[62]*VU University Amsterdam, 1081 HV Amsterdam, Netherlands*
[63]*University of Maryland, College Park, Maryland 20742, USA*
[64]*Center for Relativistic Astrophysics and School of Physics, Georgia Institute of Technology, Atlanta, Georgia 30332, USA*
[65]*Laboratoire des Matériaux Avancés (LMA), CNRS/IN2P3, F-69622 Villeurbanne, France*
[66]*Université Claude Bernard Lyon 1, F-69622 Villeurbanne, France*
[67]*Universitat de les Illes Balears, IAC3-IEEC, E-07122 Palma de Mallorca, Spain*
[68]*Università di Napoli "Federico II," Complesso Universitario di Monte S.Angelo, I-80126 Napoli, Italy*
[69]*NASA/Goddard Space Flight Center, Greenbelt, Maryland 20771, USA*
[70]*Canadian Institute for Theoretical Astrophysics, University of Toronto, Toronto, Ontario M5S 3H8, Canada*
[71]*Tsinghua University, Beijing 100084, China*
[72]*University of Michigan, Ann Arbor, Michigan 48109, USA*
[73]*National Tsing Hua University, Hsinchu City, 30013 Taiwan, Republic of China*
[74]*Charles Sturt University, Wagga Wagga, New South Wales 2678, Australia*
[75]*University of Chicago, Chicago, Illinois 60637, USA*
[76]*Caltech CaRT, Pasadena, California 91125, USA*
[77]*Korea Institute of Science and Technology Information, Daejeon 305-806, Korea*
[78]*Carleton College, Northfield, Minnesota 55057, USA*
[79]*Università di Roma "La Sapienza," I-00185 Roma, Italy*
[80]*University of Brussels, Brussels 1050, Belgium*
[81]*Sonoma State University, Rohnert Park, California 94928, USA*
[82]*Texas Tech University, Lubbock, Texas 79409, USA*
[83]*Cardiff University, Cardiff CF24 3AA, United Kingdom*
[84]*University of Minnesota, Minneapolis, Minnesota 55455, USA*
[85]*The University of Melbourne, Parkville, Victoria 3010, Australia*
[86]*The University of Texas Rio Grande Valley, Brownsville, Texas 78520, USA*
[87]*The University of Sheffield, Sheffield S10 2TN, United Kingdom*
[88]*Università di Trento, Dipartimento di Fisica, I-38123 Povo, Trento, Italy*
[89]*INFN, Trento Institute for Fundamental Physics and Applications, I-38123 Povo, Trento, Italy*
[90]*Montclair State University, Montclair, New Jersey 07043, USA*
[91]*The Pennsylvania State University, University Park, Pennsylvania 16802, USA*
[92]*National Astronomical Observatory of Japan, 2-21-1 Osawa, Mitaka, Tokyo 181-8588, Japan*
[93]*School of Mathematics, University of Edinburgh, Edinburgh EH9 3FD, United Kingdom*
[94]*Indian Institute of Technology, Gandhinagar Ahmedabad Gujarat 382424, India*
[95]*Institute for Plasma Research, Bhat, Gandhinagar 382428, India*
[96]*University of Szeged, Dóm tér 9, Szeged 6720, Hungary*
[97]*Embry-Riddle Aeronautical University, Prescott, Arizona 86301, USA*
[98]*Tata Institute of Fundamental Research, Mumbai 400005, India*
[99]*INAF, Osservatorio Astronomico di Capodimonte, I-80131 Napoli, Italy*
[100]*American University, Washington, D.C. 20016, USA*
[101]*University of Massachusetts-Amherst, Amherst, Massachusetts 01003, USA*
[102]*University of Adelaide, Adelaide, South Australia 5005, Australia*
[103]*West Virginia University, Morgantown, West Virginia 26506, USA*
[104]*University of Białystok, 15-424 Biał ystok, Poland*
[105]*SUPA, University of Strathclyde, Glasgow G1 1XQ, United Kingdom*
[106]*IISER-TVM, CET Campus, Trivandrum Kerala 695016, India*
[107]*Northwestern University, Evanston, Illinois 60208, USA*
[108]*Institute of Applied Physics, Nizhny Novgorod 603950, Russia*
[109]*Pusan National University, Busan 609-735, Korea*
[110]*Hanyang University, Seoul 133-791, Korea*

[111]*NCBJ, 05-400 Świerk-Otwock, Poland*
[112]*IM-PAN, 00-956 Warsaw, Poland*
[113]*Rochester Institute of Technology, Rochester, New York 14623, USA*
[114]*Monash University, Victoria 3800, Australia*
[115]*Seoul National University, Seoul 151-742, Korea*
[116]*University of Alabama in Huntsville, Huntsville, Alabama 35899, USA*
[117]*ESPCI, CNRS, F-75005 Paris, France*
[118]*Università di Camerino, Dipartimento di Fisica, I-62032 Camerino, Italy*
[119]*Southern University and A&M College, Baton Rouge, Louisiana 70813, USA*
[120]*College of William and Mary, Williamsburg, Virginia 23187, USA*
[121]*Instituto de Física Teórica, University Estadual Paulista/ICTP South American Institute for Fundamental Research, São Paulo São Paulo 01140-070, Brazil*
[122]*University of Cambridge, Cambridge CB2 1TN, United Kingdom*
[123]*IISER-Kolkata, Mohanpur, West Bengal 741252, India*
[124]*Rutherford Appleton Laboratory, HSIC, Chilton, Didcot, Oxon OX11 0QX, United Kingdom*
[125]*Whitman College, 345 Boyer Avenue, Walla Walla, Washington 99362, USA*
[126]*National Institute for Mathematical Sciences, Daejeon 305-390, Korea*
[127]*Université de Lyon, F-69361 Lyon, France*
[128]*Hobart and William Smith Colleges, Geneva, New York 14456, USA*
[129]*Janusz Gil Institute of Astronomy, University of Zielona Góra, 65-265 Zielona Góra, Poland*
[130]*Andrews University, Berrien Springs, Michigan 49104, USA*
[131]*Università di Siena, I-53100 Siena, Italy*
[132]*Trinity University, San Antonio, Texas 78212, USA*
[133]*University of Washington, Seattle, Washington 98195, USA*
[134]*Kenyon College, Gambier, Ohio 43022, USA*
[135]*Abilene Christian University, Abilene, Texas 79699, USA*

[†]Deceased.